Jack Francis
Department of Industrial and Systems Engineering,
Mississippi State University,
Starkville, MS 39762
e-mail: jf881@msstate.edu

Arman Sabbaghi
Department of Statistics,
Purdue University,
West Lafayette, IN 47907
e-mail: sabbaghi@purdue.edu

M. Ravi Shankar
Department of Industrial Engineering,
Swanson School of Engineering,
University of Pittsburgh,
Pittsburgh, PA 15261
e-mail: ravishm@pitt.edu

Morteza Ghasri-Khouzani
Department of Industrial Engineering,
Swanson School of Engineering,
University of Pittsburgh,
Pittsburgh, PA 15261
e-mail: ghasrikh@ualberta.ca

Linkan Bian[1]
Department of Industrial and Systems Engineering,
Center for Advanced Vehicular Systems,
Mississippi State University,
Starkville, MS 39762
e-mail: bian@ise.msstate.edu

Efficient Distortion Prediction of Additively Manufactured Parts Using Bayesian Model Transfer Between Material Systems

Distortion in laser-based additive manufacturing (LBAM) is a critical issue that adversely affects the geometric integrity of additively manufactured parts and generally exhibits a complicated dependence on the underlying material. The differences in properties between distinct materials prevent the immediate application of a distortion model learned for one material to another, which introduces the challenge in LBAM of learning a distortion model for a new material system given past experiments. Current methods for investigating the distortion of different material systems typically involve finite element analysis or a large number of experiments in an empirical study. However, these methods do not learn from previous experiments and can incur significant costs in terms of computation, time, or resources. We propose a Bayesian model transfer methodology that is both physics-based and data-driven to leverage past experiments on previously studied material systems for more efficient distortion modeling of new systems. This method transfers distortion models across distinct materials based on the statistical effect equivalence framework by formulating the differences between two materials as a lurking variable. Our method reduces the experimentation and effort needed for specifying distortion models for new material systems. We validate our methodology in a case study of distortion model transfer from Ti–6Al–4V disks to 316L stainless steel disks. This case study is the first instance of model transfer between material systems and illustrates the ability of the Bayesian model transfer methodology to address the issue of comprehensive distortion modeling across varying material systems in LBAM. [DOI: 10.1115/1.4046408]

Keywords: additive manufacturing, laser processes, transfer learning, distortion

1 Introduction

The objective of this work is to develop a model transfer framework that is both physics-based and data-driven for sharing process-related information across distinct material systems in laser-based additive manufacturing (LBAM). Our methodology provides a new approach to specify process-property models for key process outcome variables of material systems in LBAM with reduced experimentation. Specifying statistical models for key outcome variables is an important objective, because the differences in material properties (e.g., melting point, strength, and thermal conductivity) make the selection of optimum process inputs difficult. Statistical models provide a path for the selection of optimum process inputs with reduced experimentation. Currently, if a practitioner aims to predict the outcomes of parts manufactured using new materials in LBAM and identify the inputs that can optimize the outcome, then they would need to conduct a large number of trial and error experimental studies separately for each material to obtain their corresponding process-property models. Our methodology can fill the gap for the efficient establishment of input–outcome relationships in new material systems by leveraging data and other information (e.g., prior information and other sources of information besides observed data) from similar experiments involving different materials that were previously studied and modeled. This is expected to significantly reduce the time and effort needed for material certification and product development.

In this article, the distortion of a part manufactured under LBAM is taken as the key outcome variable. Distortion is the geometric difference in the z direction between the original part design and the fabricated part. Current approaches to model and predict distortion for new material systems typically involve finite element analysis (FEA) and/or empirical studies and are reviewed in Sec. 2.2. Although these approaches can provide real-world insights into the behaviors of materials, they typically require multiple experiments to yield conclusive results on different material systems, which incurs significant costs of time and effort on the part of LBAM users. Conducting full-scale empirical studies for each material and manufacturing system is not feasible due to the high costs of materials and machine operation.

Our proposed methodology for transferring models between distinct material systems addresses this challenge via three key steps. The first step is to specify a "baseline" outcome model that incorporates the relationships between observed input process variables and the outcome under a particular choice of material. In the second step, the established baseline model for the first type of material is used in combination with data on *a small sample* of parts manufactured using a new material to infer and model the total equivalent amount (TEA) of the lurking variables and properties associated with the new material in terms of the observed inputs under the baseline model. The concept of the TEA was first formalized in the statistical effect equivalence framework in Ref. [1]. In contrast to that model transfer scheme, the TEA that is specified in our methodology can directly integrate potential property differences that are known a priori to be critical to predict the outcome. Furthermore, the TEA can implicitly capture the large number of varying, and complicated, material properties by considering them as a lurking variable. Finally, in the third step, the TEA model is incorporated

[1]Corresponding author.

Manuscript received July 19, 2019; final manuscript received January 27, 2020; published online February 19, 2020. Assoc. Editor: Steven Schmid.

into the baseline model to specify a model for the new material, and thereby transfer a distortion model from one material to another while accounting for lurking variables.

An illustration of this methodology is provided in Fig. 1 for a proof-of-concept case study of distortion modeling of a 316L stainless steel disk, given a baseline distortion model for Ti–6Al–4V disks. Distortion is defined for each point on the surface of a disk as the difference between the measured height of the point after the part on which it resides is removed from the build plate and the nominal height of the point in the computer-aided design (CAD) model. The latter is constant for all points on a disk as the top surface is designed to be flat. The disks are scanned using a coordinate measurement machine (CMM) to obtain their pointwise distortions. The baseline distortion model is specified to fit the distortions of the fabricated Ti–6Al–4V disks (as described in Secs. 3 and 4). An illustration of the inferred TEA of the 316L stainless steel disk in terms of an input of the baseline distortion model for Ti–6Al–4V alloy (described more formally in Secs. 3 and 4) is in Fig. 1(*c*). This inferred TEA implicitly captures lurking differences between the two material systems (e.g., in terms of their phase transformation, melting point, and other properties). Thus, the key lurking variable effect of interest is that of changing material systems on distortion. We directly incorporate the critical, physics-based parameter of thermal conductivity when modeling the TEA. This is a key to our proposed methodology because the incorporation of physics-based parameters provides an avenue for practitioners to directly incorporate domain understanding into the statistical model. Other parameters that practitioners could integrate into the TEA model include the build setup and processing parameters. By means of our physics-based and data-driven model for the TEA (described in Secs. 3 and 4), we then transfer the distortion model specified for Ti–6Al–4V alloy to 316L stainless steel and form predictions accordingly. Sample predictions obtained by means of this transferred model are in Fig. 1(*d*).

Our proposed model transfer framework for using process-related information across distinct material systems provides practitioners with three key benefits.

(1) The expected time needed for material certification and product development will be reduced due to the reduction in the number of experiments needed to understand a new material system. The cost and time reduction in material certification will lead to practitioners being able to more efficiently test new material systems for new LBAM applications, ultimately leading to greater adoption of LBAM across various industries.
(2) Our statistical modeling framework allows the direct incorporation of practitioners' domain knowledge. This will lead to higher quality distortion models that can be geared toward specific machines or process designs.
(3) Our framework provides a first step toward a more general transfer learning-based approach for other key quality characteristics, such as porosity, density, and strength. Ultimately, the general model transfer framework aligns with the objective of Industry 4.0 to have a connected workplace that improves multiple different processes through continuous learning [2].

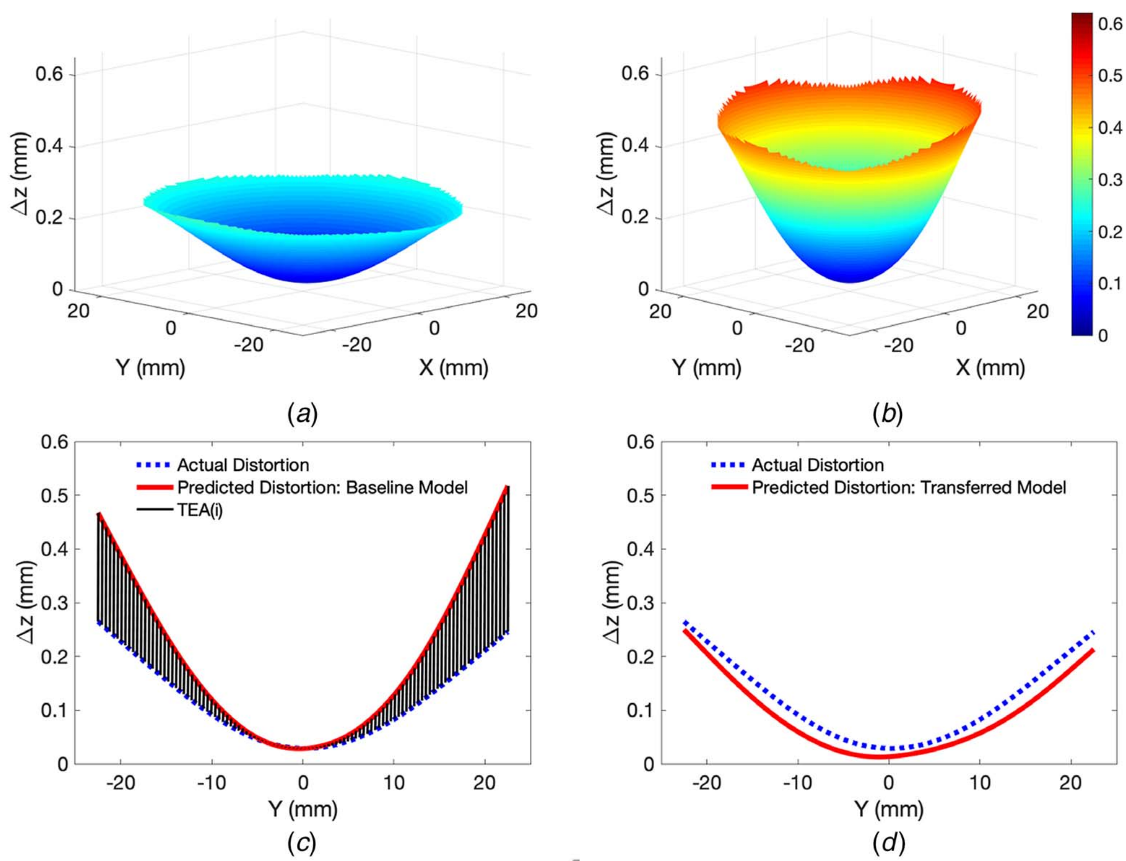

Fig. 1 **(*a*) The observed distortion (denoted by Δ*z*) of a 55 mm diameter 316L stainless steel disk under the Cartesian coordinate system. (*b*) Visualization of the predicted distortion of the 55 mm 316L stainless steel disk using the baseline distortion model that was fitted to multiple Ti–6Al–4V disks. (c) Visualization of the TEA model for the cross section of the 316L stainless steel disk that is defined by $X = 0$. The TEAs are inferred and modeled by means of a pointwise discrepancy measure between the baseline model predictions and actual distortions. (*d*) Visualization of predicted distortions from the transferred model for the same cross section of $X = 0$ when the TEA model is added to the baseline model.**

The remainder of the article is structured as follows. Section 2 contains a review of distortion in LBAM, transfer learning, and model transfer and challenges in applying transfer learning and model transfer to different materials. The Bayesian model transfer framework and baseline distortion model for Ti–6Al–4V disks are in Sec. 3. The experimental setup of the case study on Ti–6Al–4V and 316L stainless steel disks and the results of the study are in Sec. 4. Section 5 concludes with our major findings.

2 Literature Review

2.1 Material Systems and Distortion in Laser-Based Additive Manufacturing. Many studies have been conducted on distinct materials to understand how they are affected during the LBAM process [3–13]. Two of the most commonly used materials for LBAM fabrication are Ti–6Al–4V alloy and 316L stainless steel. The key benefits of these materials include their strengths at high temperatures and improved corrosion resistance. Their key differences include melting points, strengths, and thermal conductivities. Differences in thermal conductivities play a significant role in the different distortion behaviors of material systems. The thermal conductivity of Ti–6Al–4V alloy is reported as 6.7 W/(m K) [14], while that for 316L stainless steel is reported as 16.3 W/(m K) [15]. The distortion of parts manufactured using LBAM is primarily caused by large thermal gradients from the laser [16]. The continuous heating and cooling in the process leads to a build-up of residual stress, and upon the manufactured part's removal from the LBAM machine's build plate, the relaxation of residual stress introduces part distortions. The thermal conductivity of the material identifies the speed with which heating and cooling occurs for a given material. Thus, the incorporation of thermal conductivity is critical in predicting distortion. We describe in Secs. 3 and 4 how we are able to incorporate different thermal conductivities in model transfer.

2.2 Methods for Modeling and Predicting Distortion

2.2.1 Finite Element Analysis. Many research studies on distortion modeling employ finite element models to simulate the effects of thermal deformation layerwise. One example is the model developed by Roberts [17] based on the ANSYS software platform to investigate thermal and residual stresses during laser melting. Roberts found that residual stress increases as the number of layers increases for Ti–6Al–4V parts. However, this model does not scale well to large parts, and its lack of scalability due to excessive computational memory and time was identified by Paul et al. [18]. To address this issue, a modified finite element model was proposed by Paul et al. [18] (2014) that is able to predict maximum vertical thermal distortion within 7% of the model in Ref. [17]. It is based on the recognition that deformation is dominated by shrinkage of metal volume until the part cools, which enables an analytical deformation calculation for most of the part.

Another approach is the work by Mukherjee et al. [19] on deriving a non-dimensional thermal strain parameter ε^* using the Buckingham-π theorem to represent the maximal thermal strain. Effects of laser power and scan speed in the finite element model were also studied. This formulation led to the general results that distortion is positively correlated with large volumetric change, Ti–6Al–4V alloy has higher thermal strain than 316L stainless steel and Inconel 625 superalloy, and that low heat input per unit length yields decreased thermal distortion for Ti–6Al–4V alloy, 316L stainless steel, and Inconel 625 superalloy. The finite element model in Ref. [19] requires significant computation time (e.g., 7 min for a deposition of 1 cm), which limits its applicability for quickly learning about new materials.

Peng et al. [20] recently developed a rapid approach to predict thermal history based on a thermal circuit network (TCN) model. This reduces the number of layers needed to model heat transfer by grouping adjacent build layers into a "superlayer." In comparison with existing finite element models, the TCN model was significantly faster (e.g., over 99% faster) for the superlayer case, and its error was within 15% of the existing model. In the second part of Ref. [21], a quasi-static thermo-mechanical (QTM) model was introduced that can be used in tandem with the TCN to predict distortion for AlSi10Mg and 316L stainless steel disks. The TCN-QTM method was demonstrated to result in relative distortion prediction errors of 20% in terms of the radius of curvature for a wide range of test cases (e.g., disks, prisms, and triangular shapes). Although QTM is computationally efficient compared to traditional finite element models, it can incur significant time costs (e.g., 70 min) for larger parts (e.g., disks with thicknesses of at least 30 mm). Additionally, the models in Ref. [20] have a large percentage error (20%) in distortion prediction in terms of the radius of curvature, which may be unacceptable for the tight tolerances in LBAM.

The previously described models and methods highlight the key trade-off between computational efficiency and predictive performance in practice. Highly accurate models necessarily incur large computational costs due to the enormous number of equations that must be solved to model heat transfer. Alternatively, models that are more rapidly executable invoke assumptions (e.g., similar part designs or groupings of layers) that reduce overall accuracy.

2.2.2 Empirical Studies. Unlike FEA, empirical studies fabricate real-world parts with varying process parameters to understand their effects on part distortions. Denlinger et al. [22] studied the effects of inter-layer dwell time on the distortion of Ti–6Al–4V alloy and Inconel 625 superalloy in a direct energy deposition LBAM process. They obtained the interesting result that dwell time affects these materials differently. Specifically, as dwell time increases, the residual stress and distortion of Ti–6Al–4V alloy increase, whereas the residual stress and distortion of Inconel 625 superalloy decrease. While Denlinger et al. [22] provided key insights into the process-distortion relationship, their method was not immediately applicable to other LBAM processes due to the unique setup. The work of Dunbar et al. [16] involved the development of a "vault," attached below the substrate, for *in situ* temperature and distortion measurements for a laser-based powder bed fusion system. Based on the vault measurements, the researchers concluded that a constant scan pattern led to more distortion compared to a rotating scan pattern. The vault setup in this study was unique and specialized, which limits its immediate application to other LBAM systems for *in situ* distortion prediction. Corbin et al. [23] investigated the effect of preheating the substrate and substrate thickness on distortion. Experiments using Ti–6Al–4V on a Laser Engineered Net Shaping (LENS) machine were completed with varying substrates to identify the effect on distortion. The authors find a strong relationship between distortion and the thickness of the substrate. Surprisingly, they find that substrate preheating tends to increase distortion on thicker Ti–6Al–4V substrates. Levkulich et al. [24] performed experimental studies on the effect of varying process parameters on residual stress and distortion. The investigated process parameters included build height, scan speed, laser power, substrate condition, and build plan area. The authors find that substrate distortion increases as the substrate is thicker (similar to the finding of Ref. [23]). In addition, a number of experimental builds were completed to identify the relationship between residual stress and the previously mentioned process parameters. Ghasri-Khouzani et al. [25] performed an experimental study on the effects of thickness and diameter for the distortion and residual stress of 316L stainless steel disk-shaped parts. Over 70 disk-shaped parts were fabricated to understand the relationships between distortion and build design parameters. Ghasri-Khouzani et al. [25] concluded that disk thickness significantly affects distortion, with distortion decreasing as thickness increases. It is important to recognize that these conclusions and understanding of the process-distortion relationship for 316L stainless steel were obtained by manufacturing a large number of disks. This further highlights the need to more efficiently infer process-distortion relationships by leveraging previous studies, so as to reduce the manufacture of parts. In general, experimental studies tend to fabricate a large number of parts to understand the process-distortion relationship, which leads to prohibitively high costs for material certification.

2.3 Scope of Transfer Learning for Additive Manufacturing

2.3.1 Transfer Learning Methods. Transfer learning can provide a methodological framework for learning about new material systems in LBAM. Methods from this domain generally enable the leveraging of information collected from distinct environments by reweighing or transforming data from previously modeled settings [26]. The main benefit of transfer learning is that when one domain is expensive for inference or prediction, either in terms of resources, computation, or time, a similar, but cheaper, domain can be used to accelerate or facilitate learning in the expensive domain. One frequently used transfer learning method is TrAdaBoost [27], which generates predictions for a new environment by modifying the relative weights of data across settings at each step of a boosting algorithm, so as to identify and utilize data from those settings that are most similar to the new environment [28]. The effective application of transfer learning methods often requires a large amount of data [26,29,30]. Furthermore, the purely data-driven perspective of transfer learning ignores lurking variables and the insights on AM processes that can be obtained from them [26,31]. These features of current transfer learning methods limit their applicability for LBAM.

In the field of statistics, another transfer learning approach has been advanced under the concept of transportability or the extrapolation of experimental finding across domains that differ both in their distributions and in their inherent causal characteristics [32,33]. Transportability is formalized using causal diagrams and the do-calculus [34]. Current methods in transportability involve transport formulae for causal inference from heterogeneous data [32,33]. However, these methods primarily focus on nonparametric inference and cannot address the task of transferring more interpretable, parametric models across distinct environments. In addition, they may be limited in practice to linear structural equation models, whereas it is important to accommodate nonlinear models for real-life problems in LBAM.

2.3.2 Transfer Learning in Additive Manufacturing. Several applications in AM of methods related to transfer learning have recently been conducted. These generally focus on accelerating process optimization or transferring geometric deviation models across different settings of lurking variables in stereolithography.

An example of the first type of application is the work by Aboutaleb et al. [35] on developing a statistical framework for incorporating data from previous studies. Their framework is based on an extension of the sequential minimum energy design (SMED) developed by Joseph et al. [36] that captures the difference between previous data and current studies in a statistical distribution. This distribution is updated as studies are completed so as to explain the difference between similar studies. Three features of this framework and the corresponding method are (1) prior studies, even those with varying processing parameters, can be incorporated as initial experiments, (2) there are no limitations to individual builds, and (3) updates can be made based on batch design. An advantage of these features is that they can accelerate convergence to the optimum parameter design selection, which was verified in comparisons with full factorial designs and SMED [35]. However, the methodology in Ref. [35] is ultimately limited to finding optimum processing parameters and is not applicable to understanding process-distortion relationships across distinct materials.

A framework to transfer geometric shape deviation models across distinct AM processes was recently developed by Sabbaghi and Huang [1]. This framework is based on effect equivalence, which is a common phenomenon in manufacturing systems in which different process variables, including lurking variables, yield identical effects [37–40]. Under this framework, which we formally describe in Sec. 3.5, lurking differences in process settings are modeled using TEAs in terms of an observable input whose effect on the outcome was modeled under a previously studied process. A TEA yields the same outcome under a previous process as that observed in a new process. The utility of effect equivalence for stereolithography processes was demonstrated via several case studies [1,41,42]. In all of these works, only polymer-based parts, and either their in-plane or out-of-plane boundary deviations, were considered. However, due to the complex thermal interactions in LBAM, and the need to model the entire surface of a fabricated part (not just its boundary), it remains to be seen whether the effect equivalence framework can be used to understand process-distortion relationships across different materials in LBAM. The previous works also do not account for material differences or physics-based parameters when transferring models. Incorporating physics-based parameters for material systems (e.g., thermal conductivity) is critical due to their significant effects on distortions.

2.4 Contributions of Our Work on Distortion Model Transfer Across Materials. We extend the model transfer method in Ref. [1] so as to address the challenges introduced for predicting distortions of different material systems in LBAM. The key technical contributions of our work in this regard are summarized as follows:

(1) Our work is the first to establish an equivalency of process-distortion relationships between two distinct material systems in LBAM. The advantage of this is that it enables practitioners to more rapidly learn about new materials at a reduced cost compared to existing approaches that typically involve numerous experiments or computationally expensive FEA.
(2) Our methodology extends the framework in Ref. [1] for LBAM by generalizing the notion of the TEA to account for the entire surface of a part. Under this generalization, we are able to predict the distortion of 316L stainless steel disks on a powder-bed fusion system with a root mean squared error (RMSE) of less than 13 μm based on data from three shapes fabricated using this material and four Ti–6Al–4V disks. This predictive accuracy level meets the tolerance limits of many AM applications, including biomedical implants [43] and Deloitte-identified tolerances [44]. Details on the validation experiment are in Sec. 4.
(3) In addition to its predictive performance, our framework can also enable the incorporation of basic principles of physics. In particular, we incorporate the thermal conductivity of each material in our TEA model for distortion prediction. This enables our model to better capture the effects of material properties on final part distortions. It also stands in stark contrast to current data-driven transfer learning approaches.

3 Distortion Model Transfer for Laser-Based Additive Manufacturing Processes

3.1 Outline of the Model Transfer Procedure. Our Bayesian model transfer procedure proceeds via six steps. Details for these steps are provided in the following sections:

(1) Fabricate products using the first material system. In our case study, the first material system is Ti–6Al–4V alloy.
(2) Develop a baseline statistical distortion model for the first material system that captures the relationship between distortion and various specified inputs.
(3) Fabricate a small sample of new parts using the second material system. In our case study, the second material system is 316L stainless steel.
(4) Compute discrepancy measures utilizing the fitted baseline distortion model and data from the new material system to obtain point estimates of the TEA of the change in the

material system in terms of an input for all new parts. The concepts of effect equivalence and TEA are formally described in Sec. 3.5, and the specific discrepancy measure we utilize to yield a point estimate of the TEA is specified in Eq. (4) in Sec. 3.6.

(5) Develop a statistical model for the TEA based on the point estimates from the discrepancy measures. This TEA model is a function of the inputs utilized in distortion modeling. Further details on modeling the TEA are in Sec. 3.6.

(6) Fit the combination of the baseline model with the TEA model specified in Step 5 to data from both the previous and new material systems via Eq. (1) in Sec. 3.3 and Eq. (8) in Sec. 3.6. Our specified baseline model for Ti–6Al–4V disks is in Eq. (2) in Sec. 3.4.

The fifth step can be accomplished in part based on domain knowledge of LBAM. For example, we accomplish this in our case study in Sec. 4 by including the different thermal conductivities of the materials. The combined model in the sixth step corresponds to the transfer of the baseline model to the new material system.

3.2 Description of Distortion Data. The distortion for each point on the surface of a part is defined as the difference between the scanned height of the point and its nominal height as specified in the CAD model. We collect distortion data for additively manufactured parts using a CMM that scans the top surface of a part. Details on our CMM are in Sec. 4.1. By means of this CMM, the observed location for a point i on the surface is recorded in the point cloud format using Cartesian coordinates (x_i, y_i, z_i). The distortion for point i is then defined as $\Delta z_i = z_i - z_i^{\text{nom}}$, where z_i^{nom} is its nominal height as in the CAD model.

The parts we consider in our case study in Sec. 4 are four Ti–6Al–4V disks (Fig. 2(*a*)) and three 316L stainless steel disks. All these parts were manufactured using an EOS M290 machine. These shapes were selected due to their distortion behavior upon removal from the build plate. The disks varied in diameter, ranging from 45 mm to 70 mm (Table 1) but were all printed with a constant thickness of 5 mm and designed in their CAD models to have a flat top surface. These particular 316L stainless steel disks were chosen because their nominal diameters correspond to the range of the Ti–6Al–4V disks' diameters, which prevents extrapolation errors due to disk size in our distortion model transfer.

Examples of raw and preprocessed point cloud data for a single disk are in Figs. 2(*b*) and 2(*c*), respectively. We note from the latter figure that a manufactured disk will resemble a bowl upon removal from the build plate, i.e., its distortion increases monotonically from the center of the disk to the boundary. This is due to the residual stress gradient from the disk center to the boundary [25].

The number of measured, sampled points for the manufactured disks are in Table 1. Some disks had fewer sampled points than

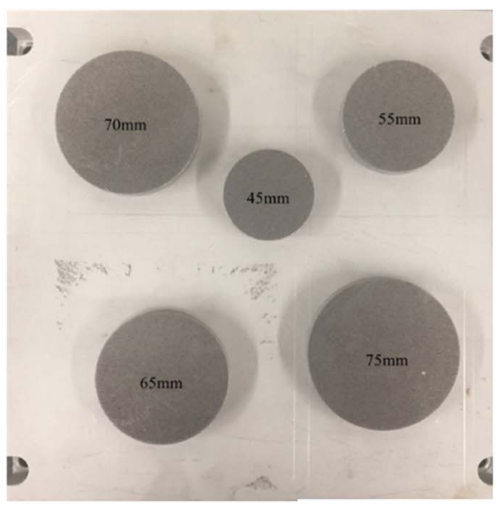

(*a*)

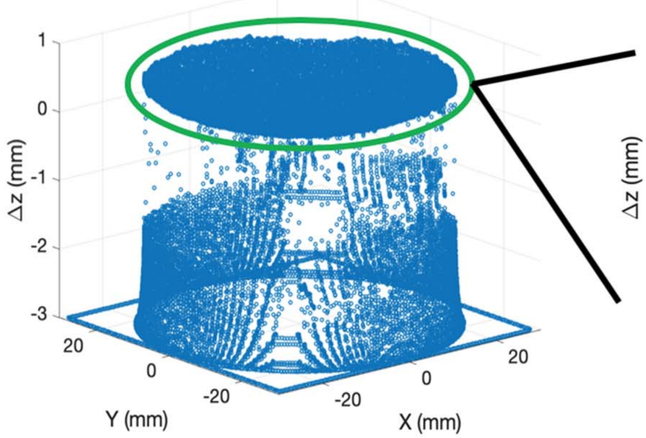

(*b*)

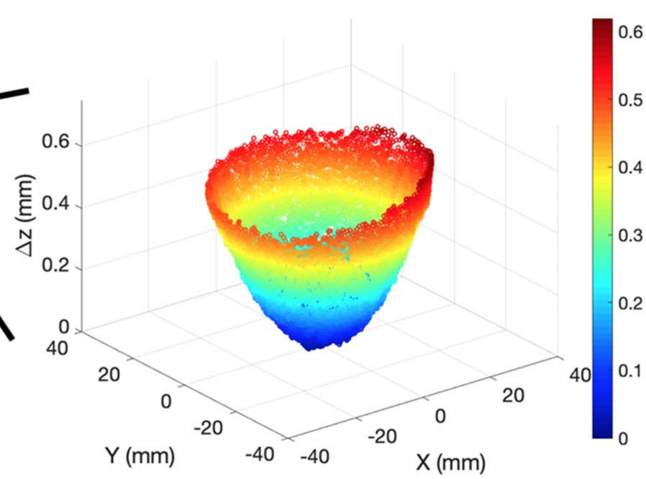

(*c*)

Fig. 2 (*a*) Build plate locations of the disks manufactured using Ti–6Al–4V alloy. (*b*) Raw point cloud data for a Ti–6Al–4V disk. The data that comprise the top surface of the disk are circled. (c) A zoomed-in view of the top surface data after pruning. Points near the disk boundary that are suspected to be plagued by severe measurement error, or that capture the underlying support structure, have been removed.

Table 1 Number of sampled points for each disk

Material	Nominal diameter (mm)	Number of sampled points
Ti–6Al–4V alloy	45	1.4×10^4
Ti–6Al–4V alloy	55	2.3×10^4
Ti–6Al–4V alloy	65	3.1×10^4
Ti–6Al–4V alloy	70	3.3×10^4
316L stainless steel	55	3.5×10^4
316L stainless steel	65	4.8×10^4
316L stainless steel	70	4.4×10^4

others due to the occurrence of increased measurement error near their boundaries that necessitated additional preprocessing of the point cloud data prior to the analyses. For disk-shaped products, part distortion leads to a shrinkage in the diameter of the part compared to the nominal diameter in the CAD model. Thus, the CMM will likely capture points that do not reside on the top surface. The preprocessing technique we utilized to account for this was data pruning, and further details on it are in Sec. 4.2.

3.3 Input Variables and Assumptions for Statistical Distortion Models. The input variables for a particular point in our statistical distortion models include any function of its location (x_i, y_i), characteristics of the design for the part on which it resides, and observed settings for the LBAM process under which it was manufactured. We denote the vector of K input variables for a point i as $w_i = (w_{i,1}, \ldots, w_{i,K})$, and let $\mathcal{W}_k$ denote the set of possible values for input $k = 1, \ldots, K$. Inputs are chosen according to their abilities to predict distortion. There exist at least two key approaches to identify necessary inputs for a distortion model: (1) scatter plot visualizations of candidate inputs with distortion. Such plots enable one to assess the strength of the correlations and trends of the variables. (2) Incorporation of physics-based parameters that have a known relationship with distortion and that are a function of the location, part design, or LBAM process parameters.

Three inputs considered in our case studies are $w_{i,1} = r_i^2$, $w_{i,2} = \theta_i$, and $w_{i,3} = d_i$, where r_i is the radius and θ_i is the angle for point i under the polar coordinate transformation of (x_i, y_i), and d_i is the nominal diameter of the disk. Note that r_i here captures the distance of point i from the center of the disk and is distinct from the nominal diameter d_i in general. All surface points are uniquely identified under the polar coordinate transformation. The strong correlations between the distortions of Ti–6Al–4V disks and r_i^2 are illustrated in Figs. 3 and 4(*a*). Figure 4(*b*) demonstrates the importance of including θ_i for distortion modeling. We also observe from Figs. 3 and 4(*a*) that the distortion for a point i is a function not only of r_i^2 but also of the nominal diameter d_i of the disk on which it resides. In particular, Fig. 4(*a*) demonstrates that for a fixed squared radius, distortion generally decreases as disk diameter increases. Furthermore, Fig. 5 illustrates how points closer to the edge of a disk have higher distortions compared to points in the middle. These observations indicate that the new input r_i^2/d_i^2, which captures the position of a point relative to the nominal diameter of its disk, may play a significant role in a distortion model.

Our selection of inputs can also be motivated by the functional approach of Huang et al. [45] to model geometric inaccuracies of an additively manufactured part based on the locations of points and characteristics of CAD models. It is important to note that the method in Ref. [45] is not directly applicable for modeling distortion in LBAM. Distortion modeling for shapes that are more geometrically complex than those we consider (e.g., cubes, pyramids, and freeform shapes with sharp corners) requires additional inputs

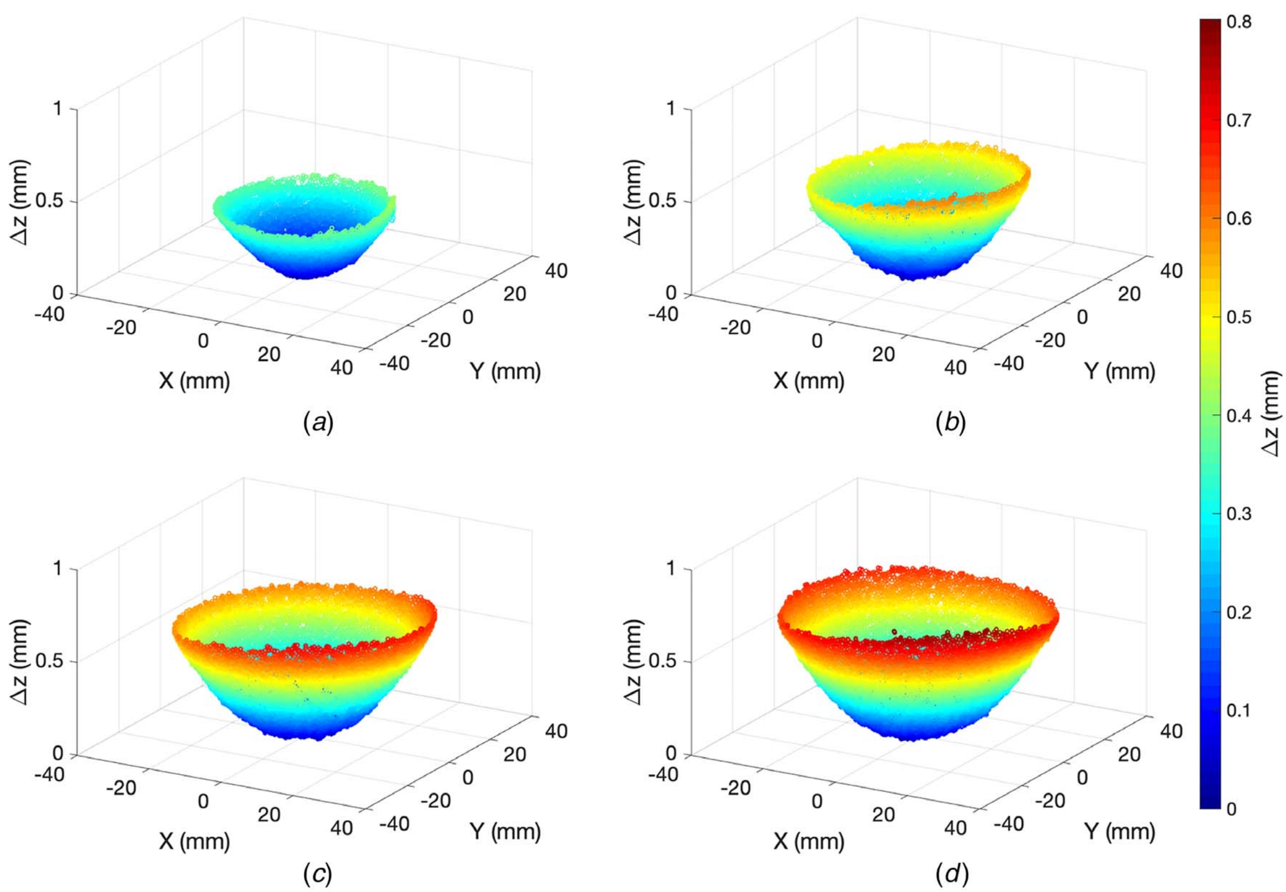

Fig. 3 Observed distortions for four Ti–6Al–4V disks of nominal diameters (*a*) 45 mm, (*b*) 55 mm, (*c*) 65 mm, and (*d*) 70 mm

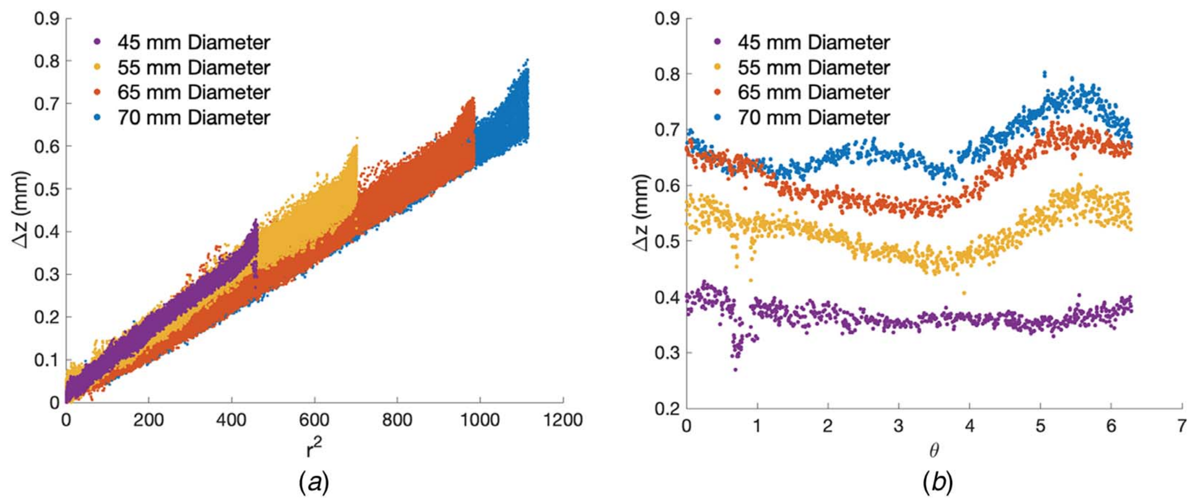

Fig. 4 (*a*) Observed distortions of points on four Ti–6Al–4V disks against their squared radii. (*b*) Observed distortions against angles for points on the boundaries (i.e., within 1.5 mm of d_i) of the parts.

that can explain the distinct distortion behaviors arising from their geometries.

We specify distortion models for distinct LBAM processes that have the same set of K inputs and satisfy two assumptions. First, a set of observed inputs $\mathcal{P} \subseteq \{1, \ldots, K\}$ can have their values change within each process. In our context, these inputs are r_i^2, θ_i, and d_i. Second, the settings of the remaining inputs are fixed within each individual process and can differ across processes. This assumption is important for the consideration of lurking variables, the settings of which are completely unobserved due to infeasibility of measurement or insufficient knowledge, and which significantly impact geometric accuracy of additively manufactured parts [1]. Statistical models are generally specified under fixed settings of lurking variables. Under these assumptions, our distortion model

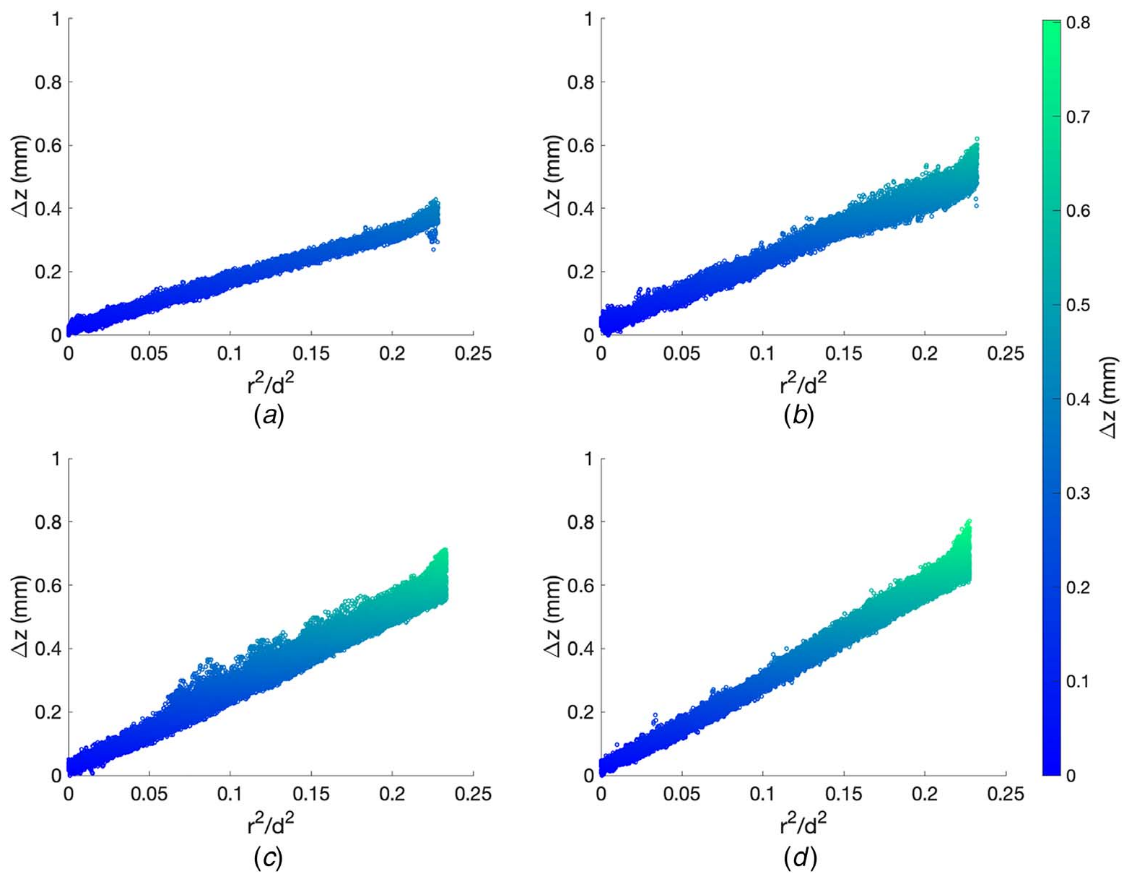

Fig. 5 Scatter plots of distortions against the positions of points relative to the nominal diameter of the disks on which they reside (denoted by r^2/d^2) for four Ti–6Al–4V disks of nominal diameters (*a*) 45 mm, (*b*) 55 mm, (*c*) 65 mm, and (*d*) 70 mm

specification for a process is

$$\Delta z_i = f_{\mathcal{P}}\big(w_{i,\mathcal{P}} \mid \beta_{\mathcal{P}}\big) + \epsilon_i \tag{1}$$

where $f_{\mathcal{P}}\big(w_{i,\mathcal{P}} \mid \beta_{\mathcal{P}}\big)$ is the expected distortion of a point i, vector $w_{i,\mathcal{P}}$ contains the values for the inputs in $\mathcal{P}$ for point i, the settings of the remaining inputs are held fixed for the process that manufactured the part on which point i resides, $\beta_{\mathcal{P}}$ is the vector of (unknown) model parameters for $f_{\mathcal{P}}$, and ϵ_i are random variables representing measurement error. We assume $\epsilon_i \sim \mathrm{N}(0, \sigma^2)$ independently.

3.4 Baseline Distortion Model Specification. Our model transfer methodology is performed with respect to a specified distortion model for a previous LBAM process with fixed settings of inputs $\{1, \ldots, K\} - \mathcal{P}$. This model is referred to as the baseline distortion model. In our context, the Ti–6Al–4V alloy material system constitutes the fixed settings of the remaining inputs (including lurking variables) under which we specify a baseline distortion model. In general, when defining the baseline model, practitioners should use inputs that (1) predict the process-distortion relationship and (2) allow for the explainability of the geometry of the fabricated part. The former can be identified using scatter plots or a practitioner's domain knowledge. The latter allows for the specification of a model in which part geometry plays a significant role in the resulting distortion, such as for a freeform shape with sharp corners and cavities. The form of $f_{\mathcal{P}}\big(w_{i,\mathcal{P}} \mid \beta_{\mathcal{P}}\big)$ that we adopt for the Ti–6Al–4V alloy baseline model is motivated by Figs. 3–5 as

$$\begin{aligned} f_{\mathcal{P}}\big(w_{i,\mathcal{P}} \mid \beta_{\mathcal{P}}\big) = \beta_0 + \beta_1 r_i^2 + \beta_2(d_i - 60) \\ + \beta_3(d_i-60)^2 + \beta_4\left(\frac{r_i^2}{d_i^2}\right) + \beta_5 h_i \\ + \beta_6(d_i-60)h_i + \beta_7(d_i-60)^2 h_i \end{aligned} \tag{2}$$

where

$$\begin{aligned} h_i = \Big[\mathbb{I}(d_i = 45)\cos\big(\theta_i - \psi_{45}\big) + \mathbb{I}(d_i = 55)\cos\big(\theta_i - \psi_{55}\big) \\ + \mathbb{I}(d_i = 65)\cos\big(\theta_i - \psi_{65}\big) + \mathbb{I}(d_i = 70)\cos\big\{2\big(\theta_i - \psi_{70}\big)\big\} \Big] \end{aligned} \tag{3}$$

Here, $w_{i,\mathcal{P}} = (r_i^2, \theta_i, d_i)$ and $\beta_{\mathcal{P}} = (\beta_0, \beta_1, \ldots, \beta_7, \psi_{45}, \psi_{55}, \psi_{65}, \psi_{70})$. We utilize the transformation $(d_i - 60)$ of input d_i so as to obtain interpretable regression coefficients corresponding to the linear and quadratic effects of nominal diameter. Specifically, these effects are defined with respect to a disk of nominal diameter 60 mm, which lies in the middle of the range of disks considered in our case study. Furthermore, our use of this transformed input yields a model that more appropriately captures the curvilinear relationship between nominal diameter and distortion over the range of nominal diameters in our case study. Besides having interpretable linear and quadratic effects of nominal diameter, our model also entertains the possibility of an interaction between these terms and the previously described harmonic trends in distortion. The terms $\cos(\theta_i - \psi_{45})$, $\cos(\theta_i - \psi_{55})$, $\cos(\theta_i - \psi_{65})$, and $\cos\{2(\theta_i - \psi_{70})\}$ are introduced to account for possible differences in the harmonic trends of distortion (Fig. 4(*b*)). These differences may be due to inconsistent definitions of starting locations that were adopted when the disks were scanned. The angle shift parameters ψ_{45}, ψ_{55}, ψ_{65}, and ψ_{70} are unique to each disk. This baseline distortion model performs well for the Ti–6Al–4V disks, with a RMSE within 20 μm. Further details on the model fit are in Sec. 4.3.

3.5 Distortion Model Transfer via Mean Effect Equivalence. We develop a model transfer framework based on the method in Ref. [1] for our transfer of a baseline distortion model to another LBAM process characterized by a distinct material system. To facilitate the description of our framework, we consider the case of $K = 2$ in the following definition.

Definition 1. *Inputs* 1 *and* 2 *are equivalent with respect to the mean if for any point i and fixed settings* $c_1 \in \mathcal{W}_1$ *and* $c_2 \in \mathcal{W}_2$, *functions* $T_{i,1\to 2}\colon \mathcal{W}_1 \times \mathcal{W}_2 \to \mathcal{W}_2$ *and* $T_{i,2\to 1}\colon \mathcal{W}_1 \times \mathcal{W}_2 \to \mathcal{W}_1$ *exist such that for all* $(w_1, w_2) \in \mathcal{W}_1 \times \mathcal{W}_2$

$$f_{\{1,2\}}\big((w_1, w_2) \mid \beta_{\{1,2\}}\big) = f_{\{2\}}\big(T_{i,1\to 2}(w_1, w_2) \mid \beta_{\{2\}}\big)$$

$$f_{\{1,2\}}\big((w_1, w_2) \mid \beta_{\{1,2\}}\big) = f_{\{1\}}\big(T_{i,2\to 1}(w_1, w_2) \mid \beta_{\{1\}}\big)$$

where

- $f_{\{1,2\}}$ *is the expected distortion under any values* w_1 *and* w_2 *of inputs* 1 *and* 2, *respectively, with parameter vector* $\beta_{\{1,2\}}$,
- $f_{\{2\}}$ *is the expected distortion under any value of input* 2 *when the value of input* 1 *is held fixed at* c_1, *with parameter vector* $\beta_{\{2\}}$, *and*
- $f_{\{1\}}$ *is the expected distortion under any value of input* 1 *when the value of input* 2 *is held fixed at* c_2, *with parameter vector* $\beta_{\{1\}}$.

To explain the notation in Definition 1 for our context, let input 1 be r_i^2, input 2 be material system, and c_2 denote a baseline material system. Function $T_{i,2\to 1}$ is the TEA of the material system in terms of squared radius with respect to the mean for point i. For a single point i on an additively manufactured product, the true TEA $T_{i,2\to 1}$ can be viewed as a parameter that, once it is incorporated into a previous model, enables predictions for the point under a new setting. The TEA is an unknown quantity, and we describe in Sec. 3.6 how the fourth and fifth steps of our methodology are performed using discrepancy measures to yield point estimates and a model for the TEA. Our particular choice of TEA here can be motivated by recognizing that the bowl shape of disk distortions, as described by the relationship between Δz_i and r_i^2, changes across different materials. Furthermore, as recognized in Ref. [1], model transfer is facilitated in practice by means of equivalencies in terms of an input that enables flexible modeling. Squared radius r_i^2 is one such convenient input for distortion modeling. Thus, we consider the TEA of a material system in terms of this input. It is important to note that our use of $f_{\mathcal{P}}$ is more general than the models in Definition 1 because it incorporates more than one input.

The TEA in Definition 1 enables the transfer of the baseline distortion model to new materials. This is because the model for expected distortions under the baseline setting c_2 can be transferred to model expected distortions under a distinct material system by incorporating $T_{i,2\to 1}$ into $f_{\{1\}}$, where the effect of squared radius has been modeled in $f_{\{1\}}$ under setting c_2. Specifically, letting Δz_i denote the observed distortion for a point i under the new material system, the transferred model will be specified according to $\Delta z_i = f_{\{1\}}(T_{i,2\to 1}(w_1, w_2)|\beta_{\{1\}}) + \delta_i$, where $\delta_i \sim \mathrm{N}(0, \tau^2)$ independently and are the error terms for the new material. From this specification, we then fit a comprehensive model to data from the two material systems in the sixth step of our methodology. Data from the baseline material will be modeled according to the $\mathrm{N}(f_{\{1\}}(w_{i,1}|\beta_{\{1\}}), \sigma^2)$ statistical distribution, and data from the new material will be modeled according to the $\mathrm{N}(f_{\{1\}}(T_{i,2\to 1}(w_{i,1}, w_{i,2})| \beta_{\{1\}}), \tau^2)$ statistical distribution. These two models, and their corresponding parameters, are fit simultaneously to all of the data, with the consequence that data from the baseline material are further leveraged for fitting the transferred model for the new material. When fitting this comprehensive model, function $T_{i,2\to 1}$ essentially benchmarks the effect of input 2 on distortion in terms of a previous setting and the effect of input 1 on the mean under it [1].

3.6 Bayesian Modeling of the Total Equivalent Amount of a Material System. From Definition 1, model transfer from one material system to another can be performed when the unknown, realized TEAs of the change in material system are inferred and modeled based on the fitted baseline distortion model and data from the new material. In the fourth and fifth steps of the methodology, we utilize the Bayesian discrepancy measure approach developed in Ref. [1] to yield point estimates and a model for the unknown TEAs, respectively. We assume that the baseline model has been specified under a fixed material system, and that the posterior distribution $p(\beta_{\mathcal{P}}, \sigma^2 \mid D_1)$ for the baseline model parameters based on the data D_1 obtained from the corresponding LBAM process has been calculated. We also assume that data D_2 have been collected for a new material.

In general, to obtain a point estimate of the realized TEA for a particular point i in D_2 in terms of the chosen input $w_{i,1} = r_i^2$, we construct the discrepancy measure

$$T_i = \underset{t \in (-r_i^2, \infty)}{\operatorname{argmin}} \left\{ \Delta z_i - f_{\mathcal{P}}\left((w_{i,1} + t,\, w_{i,2},\, w_{i,3}) \mid \widetilde{\beta}_{\mathcal{P}} \right) \right\}^2 \tag{4}$$

where $\mathcal{P} = \{1, 2, 3\}$ for the baseline distortion model of Ti–6Al–4V disks, and $\widetilde{\beta}_{\mathcal{P}}$ is a random variable distributed according to the marginal posterior distribution $p(\beta_{\mathcal{P}} \mid D_1)$. From the specified baseline distortion model in Eqs. (2) and (3), the discrepancy measure for any point on a 316L stainless steel disk is the random variable

$$\begin{aligned} T_i = \underset{t \in (-r_i^2, \infty)}{\operatorname{argmin}} \Big\{ & \Delta z_i - \widetilde{\beta}_0 - \widetilde{\beta}_1 (r_i^2 + t) - \widetilde{\beta}_2 (d_i - 60) \\ & - \widetilde{\beta}_3 (d_i - 60)^2 - \widetilde{\beta}_4 \left(\frac{r_i^2 + t}{d_i^2} \right) \\ & - \widetilde{\beta}_5 \widetilde{h}_i - \widetilde{\beta}_6 (d_i - 60) \widetilde{h}_i - \widetilde{\beta}_7 (d_i - 60)^2 \widetilde{h}_i \Big\}^2 \end{aligned} \tag{5}$$

where

$$\begin{aligned} \widetilde{h}_i = \big[& \mathbb{I}(d_i = 45) \cos\left(\theta_i - \widetilde{\psi}_{45}\right) + \mathbb{I}(d_i = 55) \cos\left(\theta_i - \widetilde{\psi}_{55}\right) \\ & + \mathbb{I}(d_i = 65) \cos\left(\theta_i - \widetilde{\psi}_{65}\right) + \mathbb{I}(d_i = 70) \cos\left\{ 2\left(\theta_i - \widetilde{\psi}_{70}\right) \right\} \big] \end{aligned} \tag{6}$$

Equation (5) can be immediately solved in closed-form for each set of posterior draws of the parameters. Similar to the framework in Ref. [1], we consider the TEA as an additive component to input 1 when we perform this inference. In addition, although point estimates for TEAs in terms of any input can be performed in general, we calculate the discrepancy measure according to a minimization problem relative to only the first input variable. This is because r_i^2 possesses a more flexible capability for model transfer compared to the other inputs, in terms of capturing the change in the bowl shape of disk distortions across the two different materials. Following the general observations made in Ref. [1], obtaining point estimates for the TEAs via this random variable is computationally simpler than other Bayesian approaches, such as deriving the posterior distributions of the high-dimensional TEAs. Discrepancy measures are a type of posterior predictive check [46–48] and have proven to be effective for learning about unknown quantities in previous additive manufacturing studies [1,41,45,49,50]. Also, point estimates obtained via Eq. (4) will in general be similar to those obtained by means of the posterior distributions of the TEAs [1].

After we obtain the distributions of the T_i, we examine summaries of them to specify our model for the realized TEAs under the second setting as a function of the other observable inputs. The specific summary we examine for each point i is the average value of its discrepancy measure distribution. If we let $p(T_i)$ denote the probability density function of T_i, as derived by the representation of this random variable in Eq. (4), then this average value is $\int_{-r_i^2}^{\infty} T_i p(T_i) dT_i$. In practice, we approximate this integral using draws $T_i^{(l)}$ generated from the probability density function $p(T_i)$ according to the combination of Eq. (4) with draws $\beta_{\mathcal{P}}^{(l)}$ from the posterior distribution $p(\beta_{\mathcal{P}} \mid D_1)$, where $l = 1, \ldots, L$ indexes the draws. It is important to note that each $T_i^{(l)}$ is constructed according to a single corresponding draw $\beta_{\mathcal{P}}^{(l)}$. The mean value of the discrepancy measure does not equal the true, unknown TEA but instead corresponds to one particular point estimator of the TEA. In large samples, the variability of this point estimator should be negligible, and the mean value of the discrepancy measure should approximate the TEA.

We denote the specified TEA model as $T(w_{i,\mathcal{P}} \mid \gamma)$, where γ denotes the (unknown) vector of model parameters. The TEA model can involve functions of the entries in w_i besides just $w_{i,1}$, which are viewed as covariates. For example, the difference in thermal conductivities between a new material and the baseline material can enter as a linear effect in the TEA model and has a corresponding parameter γ_0 in the γ vector. It is in this way that, unlike the previous work in Ref. [1], our TEA model allows for the direct incorporation of physics-based parameters. This fact will play an important role in our case study in Sec. 4, in which the TEA will be modeled as a polynomial function of r_i^2, $\cos(\theta_i)$, $\sin(\theta_i)$, d_i, and the difference in the thermal conductivities of Ti–6Al–4V alloy and 316L stainless steel. As the TEA model is a function of inputs to best fit the calculated mean values of the discrepancy measures, it will not necessarily be equivalent to the mean values. Furthermore, the TEA model approximates the relationship between the true, unknown TEAs and the input variables in large samples but again is not necessarily equivalent to the TEAs because it is specified according to observed data. We summarize all of our previous notes on the TEAs, the discrepancy measures, and the TEA model by the equation

$$T_{i,2\to 1} \approx \int_{-r_i^2}^{\infty} T_i p(T_i) dT_i \approx T(w_{i,\mathcal{P}} | \gamma) \text{ for each data point } i \tag{7}$$

Model transfer to the new setting will be complete upon incorporating $T(w_{i,\mathcal{P}} \mid \gamma)$ into $f_{\mathcal{P}}$ to obtain the model

$$\Delta z_i = f_{\mathcal{P}}\left(\left(w_{i,1} + T\left(w_{i,\mathcal{P}} \mid \gamma\right),\, w_{i,2},\, w_{i,3} \right) \mid \beta_{\mathcal{P}} \right) + \delta_i \tag{8}$$

for each point i in the new setting, with $\delta_i \sim \mathrm{N}(0, \tau^2)$ independently, and where the error terms associated with the two settings are mutually independent. The results of this model transfer are described in Secs. 4.4 and 4.5.

4 Case Study of Distortion Model Transfer From Ti–6Al–4V to 316L Stainless Steel

4.1 Detailed Experimental Setup. Four Ti–6Al–4V disks and three 316L stainless steel disks were manufactured for our case study. The disks varied in diameter, ranging from 45 mm to 70 mm, but were printed with a constant thickness of 5 mm and designed to have a flat top surface in their CAD models. The locations of the Ti–6Al–4V disks in the build are in Fig. 2(*a*). The build setup for the 316L stainless steel disks differed from that for the Ti–6Al–4V disks. The optimized process parameters that were implemented when manufacturing the disks, as suggested by EOS, are in Table 2. Ultra-high purity argon gas was purged into the build chamber to ensure that the oxygen level remained below 0.1%. To further reduce distortion, all samples were printed on block style support structures generated via Materialise Magics. The Renishaw

Table 2 Optimized process parameters for the EOS M290 machine that were used to manufacture the disks

Process parameters	Ti–6Al–4V alloy	316L stainless steel
Layer thickness	30 μm	20 μm
Laser power	170 W	195 W
Scan speed	1200 mm/s	1083 mm/s
Hatch spacing	100 μm	80 μm
Build plate temperature	35 °C	80 °C

Cyclone Series 2 CMM was used to collect the disks' point cloud surface measurements, and distortions, upon removal from the build plate. This CMM has a 1 μm position resolution and an axial repeatability of ± 2 μm. Contact scanning was performed using a touch-trigger probe with a 3 mm tip diameter. RENISHAW TRACECUT 24A software was used for the acquisition of the point cloud data.

4.2 Data Preprocessing. As illustrated in Fig. 2(*b*), the point cloud data generated from the CMM for each of the fabricated disks are dense. We obtained genuine representations of the large amount of distortion data captured by the CMM, excluding measurements from the scan of the plate and support structures that are not of interest, by pruning the recorded point clouds. This was performed systematically and consistently via two steps. First, all points beyond the boundary (i.e., the diameter) of a disk, and all points within a short distance of the boundary (which depends on the nominal diameter), were removed. The latter set of points were removed because distortion led to the true diameters of the disks being smaller than their nominal diameters. Smaller boundary regions were cutoff for smaller disks compared to larger disks, because the former distorted less overall than the latter. All disks, excluding the 65 mm and 70 mm Ti–6Al–4V disks, had a cutoff value of 1 mm. Cutoff values of 1.1 mm and 1.6 mm were used for the 65 mm and 70 mm Ti–6Al–4V disks, respectively. Second, a lower bound for the recorded z coordinates was manually identified for each disk and used to remove points on the support structure. All points on a disk whose recorded z coordinates were below the disk's lower bound were removed. The first step above helps to minimize measurement errors introduced by the CMM near the boundaries of disks, and the second removes the vast majority of points that do not truly reside on the top surface.

4.3 Fitting the Baseline Distortion Model to Ti–6Al–4V Disks. We fit the baseline distortion model in Eq. (2) to the Ti–6Al–4V disks' data under the Bayesian paradigm. We place flat priors on $\beta_0, \ldots, \beta_7$, and $\log(\sigma^2)$, Uniform priors on $[0, 2\pi]$ for ψ_{45}, ψ_{55}, and ψ_{65}, and a Uniform prior on $[0, \pi]$ for ψ_{70}. We constrain the prior distribution for ψ_{70} to $[0, \pi]$ due to our previous observation from Fig. 4(*b*) that the harmonic trend for the 70 mm disk appears to exhibit a period of π, not 2π as for the other disks. For this choice of period in our baseline model, the use of a Uniform prior on $[0, 2\pi]$ for the 70 mm disk would introduce identifiability issues when performing statistical inferences because non-zero mass would be given to values in $(\pi, 2\pi]$. All of these parameters are assumed to be independent a priori. In practice, the point cloud data collected on each part will be sufficiently large in size so that the prior distributions of $\beta_{\mathcal{P}}$ and σ^2 will not be of major concern. The joint posterior distribution of the parameters is derived by a Metropolis-Hastings-within-Gibbs algorithm. Further details on our Bayesian computations are provided in the Supplemental Material on the ASME Digital Collection. Figure 6 displays the posterior predictive means of distortions for the sampled points under our fitted Bayesian model, and Fig. 7 illustrates the residuals for our fitted model. Formal posterior summaries for the parameters and residual diagnostics are in the Supplemental Material on the ASME Digital Collection. We observe that this model provides a good fit to the distortion data of the Ti–6Al–4V disks, with a RMSE of approximately 16 μm. In addition, we fitted the model using 80% of the distortion data from the Ti–6Al–4V disks and used the remaining data for testing. The RMSE for the test set only slightly increased to 18 μm, which indicates that the baseline model does not overfit the distortion data of the Ti–6Al–4V disks. Thus, as the model captures the major associations between the inputs and distortion, and does not overfit the

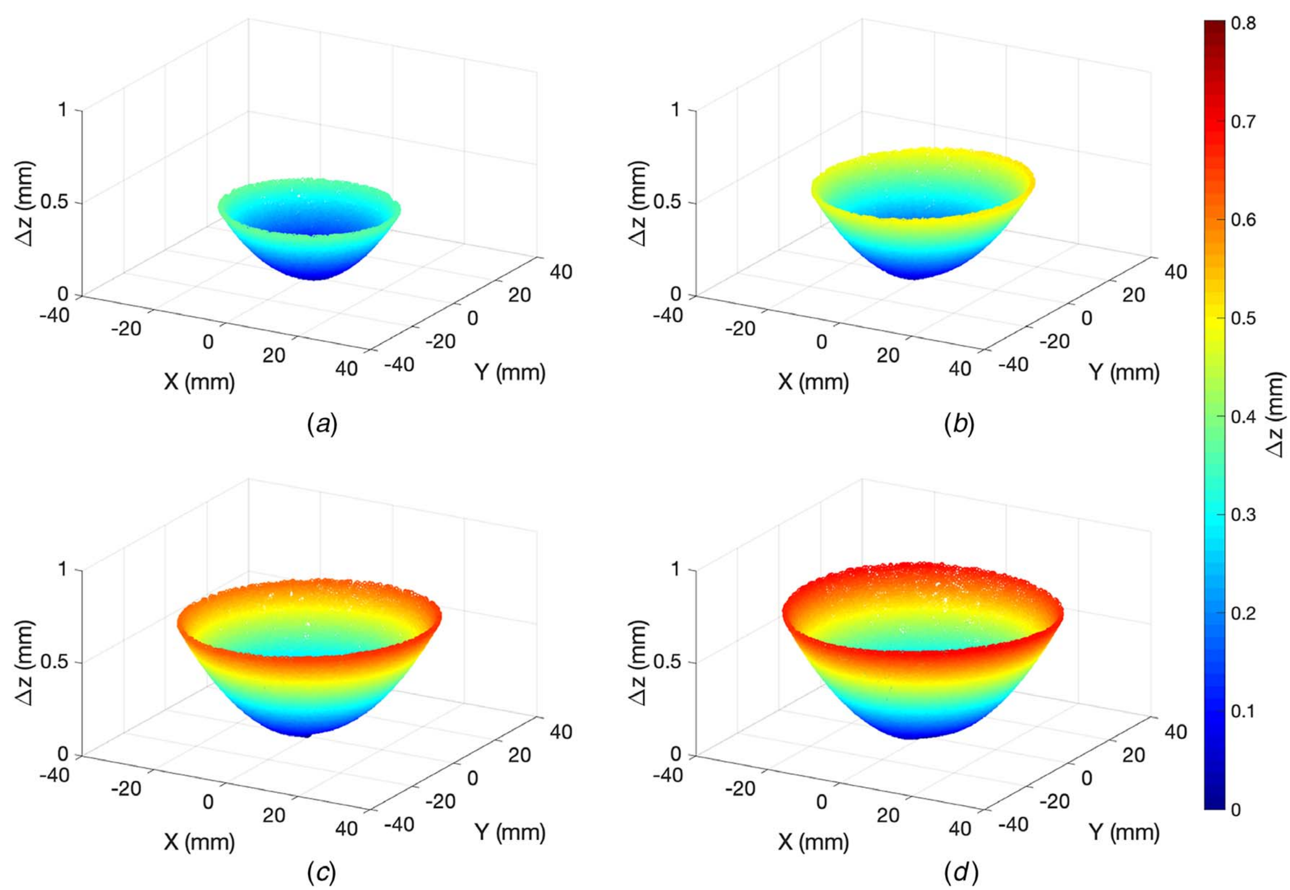

Fig. 6 Posterior predictive means of distortions for Ti–6Al–4V disks of nominal diameters (*a*) 45 mm, (*b*) 55 mm, (*c*) 65 mm, and (*d*) 70 mm, as obtained from the baseline distortion model

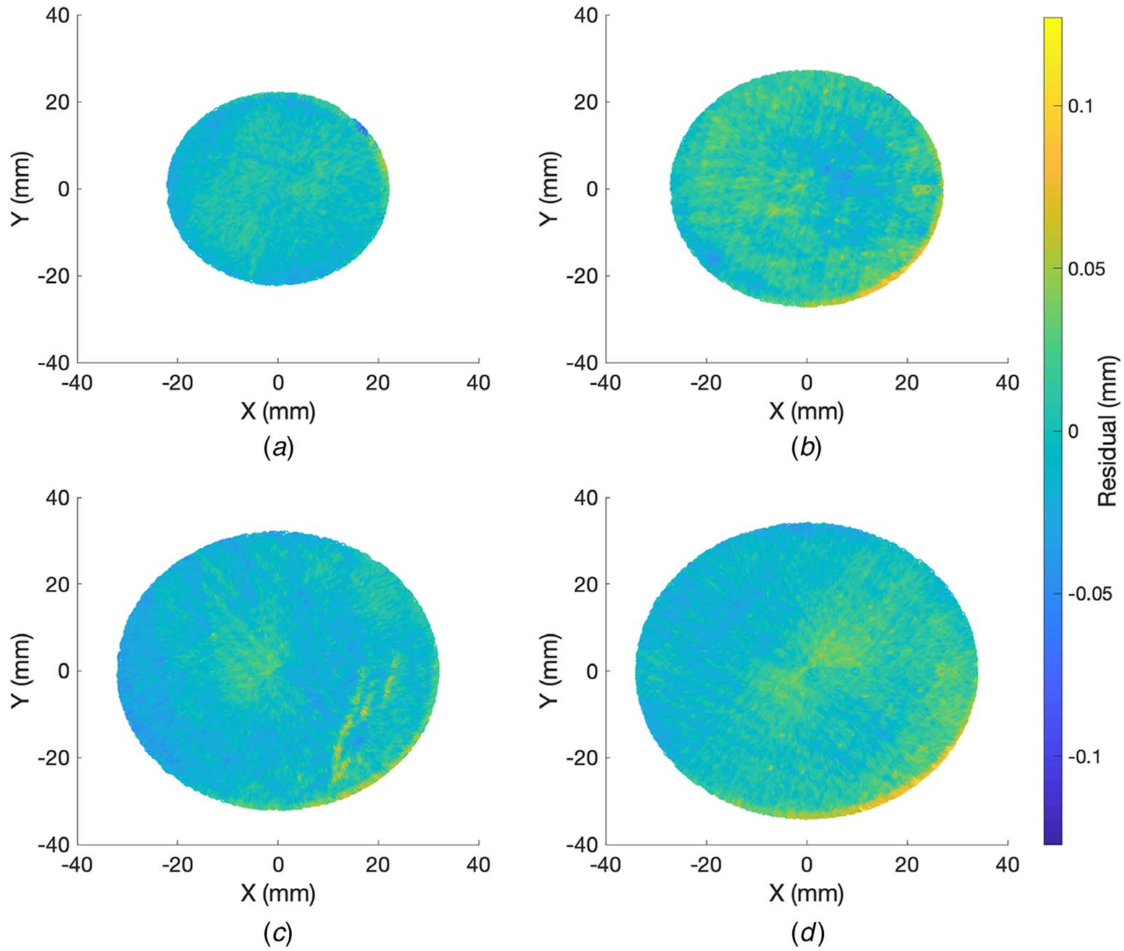

Fig. 7 Residuals for the baseline distortion model fitted to the four Ti–6Al–4V disks with a thickness of 5 mm and nominal diameters (*a*) 45 mm, (*b*) 55 mm, (*c*) 65 mm, and (*d*) 70 mm. The residual for a point is defined as the difference between its observed distortion Δz_i and the posterior predictive mean of its distortion as obtained from the baseline distortion model.

data, we will proceed to use it as the baseline model for our model transfer.

4.4 Distortion Model Transfer From Ti–6Al–4V to 316L Stainless Steel.

We proceed to use the fitted baseline distortion model for the Ti–6Al–4V disks to infer and model the realized TEAs of 316L stainless steel disks in terms of squared radius r_i^2 with respect to the mean. The distortions of the sampled points for this new material system are in Fig. 8. Three-dimensional scatter plots of the means of the discrepancy measures for these TEAs are in Fig. 9. We observe that the trends of the realized TEAs can be described in terms of location-dependent and location-independent components. The location-dependent component involves r_i^2 and θ_i and is formulated by recognizing that the inferred TEAs effectively resemble paraboloids. Accordingly, this first component is specified by the polar coordinate expression of a paraboloid. The location-independent component involves properties of the 316L stainless steel disks besides r_i^2 and θ_i. Two such important properties are nominal diameter and thermal conductivity, where the latter is directly related to the material difference between Ti–6Al–4V alloy and 316L stainless steel. Furthermore, the TEA may involve interactions between the location-dependent and location-independent components.

Our previous observations on the point estimates of the TEAs for the 316L stainless steel disks, which are the means of the discrepancy measures, lead to the following TEA model specification for a point i on a 316L stainless steel disk of nominal diameter d_i:

$$\begin{aligned}T(r_i^2, \theta_i, d_i \mid \gamma) = {} & \gamma_0(16.3 - 6.7) + \gamma_1(d_i - 65) \\ & + \gamma_2(d_i - 65)^2 + \gamma_3 r_i \cos(\theta_i) \\ & + \gamma_4 r_i^2 \cos(\theta_i)^2 + \gamma_5 r_i \sin(\theta_i) \\ & + \gamma_6 r_i^2 \sin(\theta_i)^2 + \gamma_7 r_i (d_i - 65)\cos(\theta_i) \\ & + \gamma_8 r_i^2 (d_i - 65)\cos(\theta_i)^2 + \gamma_9 r_i (d_i - 65)\sin(\theta_i) \\ & + \gamma_{10} r_i^2 (d_i - 65)\sin(\theta_i)^2\end{aligned} \tag{9}$$

where $\gamma = (\gamma_0, \ldots, \gamma_{10})$ is the vector of (unknown) parameters for the TEA model specification. The TEA model captures how the mean values of the discrepancy measure for points on the stainless steel disks are related to the input variables, such as d_i, r_i^2, and θ_i. In addition, key differences that are known a priori to exist between the materials (e.g., thermal conductivity) can be used in the TEA model to better model the mean values of the discrepancy measure. In our model, coefficient γ_0 captures the location-independent effect of changing the thermal conductivity of a disk from 6.7 W/(m K) for Ti–6Al–4V alloy to 16.3 W/(m K) for 316L stainless steel. It is in this manner that the TEA model can accommodate physically known characteristics between parts that involve multiple different materials and other lurking differences. We again utilize the transformation $(d_i - 65)$ of the input d_i in our TEA model so as to obtain interpretable regression coefficients

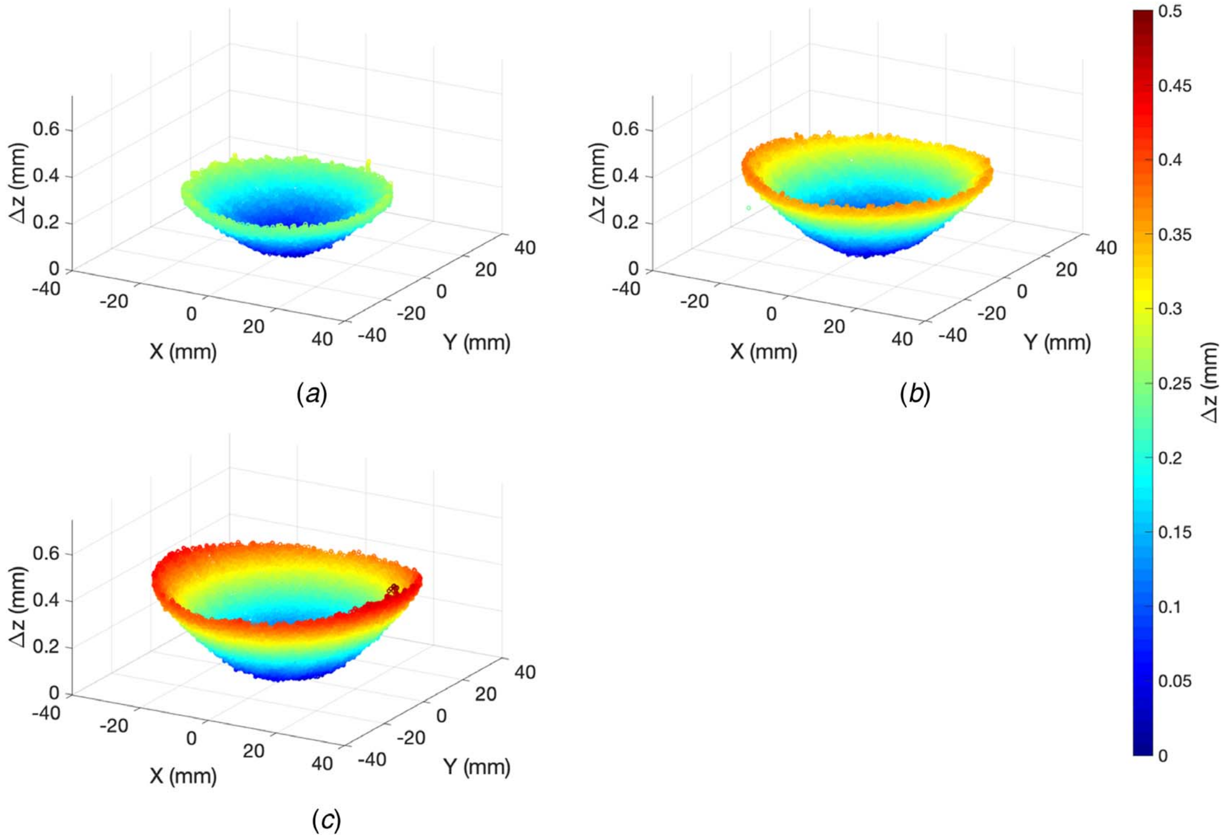

Fig. 8 Observed distortions for three 316L stainless steel disks of nominal diameters (*a*) 55 mm, (*b*) 65 mm, and (*c*) 70 mm

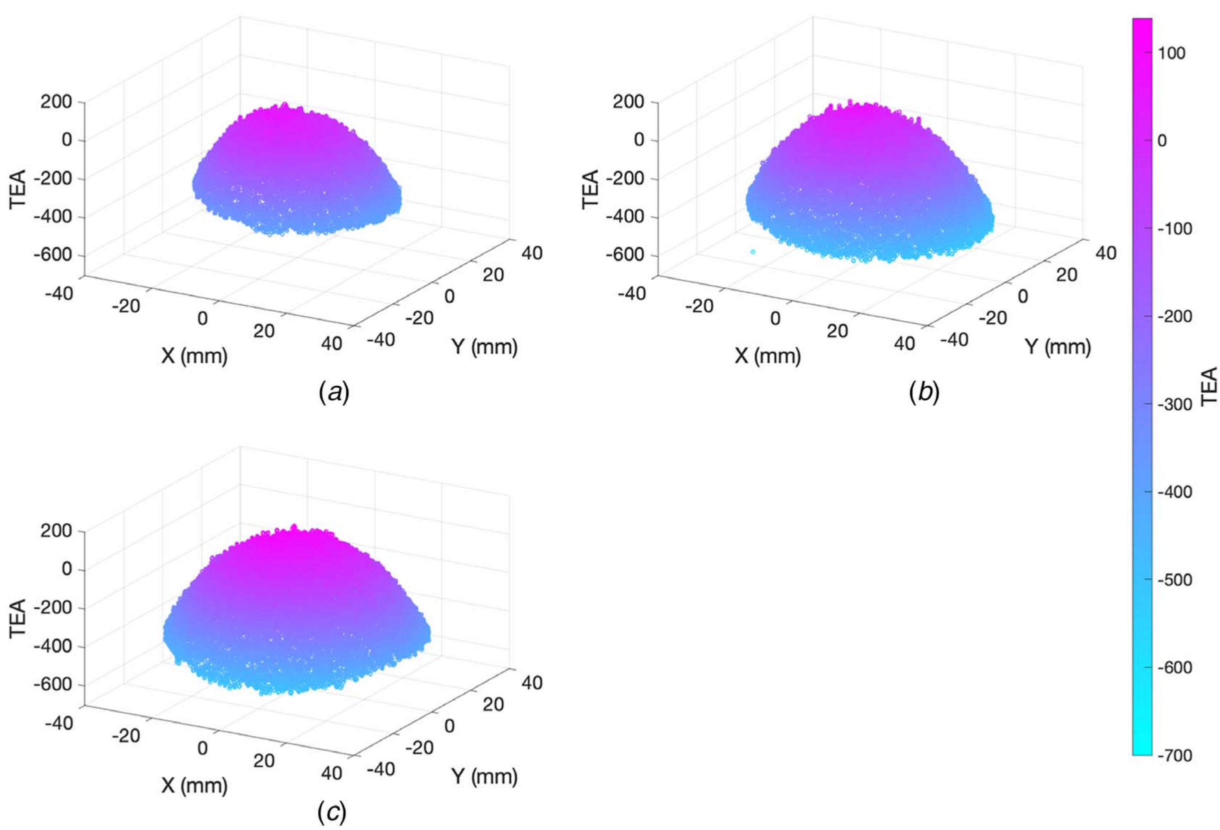

Fig. 9 Average values of the discrepancy measures that are utilized to yield point estimates of the TEAs of points on the 316L stainless steel disks of nominal diameters (*a*) 55 mm, (*b*) 65 mm, and (*c*) 70 mm

corresponding to the linear and quadratic effects of nominal diameter with respect to the range of disks considered in our case study. Furthermore, our use of this transformed input yields a TEA model that more appropriately captures the exhibited trends of the realized TEAs.

4.5 Results of the Transferred Model for 316L Stainless Steel Disks. After modeling the TEA for 316L stainless steel disks, we simultaneously fit the baseline distortion model and the transferred distortion model to the Ti–6Al–4V and 316L stainless steel disks, respectively, under the Bayesian paradigm. Independent, flat priors are placed on all of the parameters in γ. The models were fit by a Metropolis-Hastings-within-Gibbs algorithm, which is described in the Supplemental Material on the ASME Digital Collection. Formal posterior summaries for the parameters in γ and residual diagnostics are in the Supplemental Material on the ASME Digital Collection.

Distortion predictions for the 316L stainless steel disks are in Fig. 10, and the corresponding residuals for the transferred model are in Fig. 11. In Fig. 11, we note a pattern in the residual plot, specifically parallel lines of higher residuals. These larger residuals can likely be attributed to the scan pattern of the top layer. We observe from both figures that the transferred model provides a good fit to the data for this new material system. The RMSE for the transferred model is approximately 12 μm, which is lower than the RMSE of the Ti–6Al–4V disks due to the Ti–6Al–4V disks having larger distortion than 316L stainless steel disks of similar diameter, as shown in Figs. 4 and 8. To account for this, we provide in Table 3 each disk's "percent error RMSE," defined as RMSE / max (Δz_i). These values again indicate that our transferred model yields accurate fits for the disks. In addition, each value is below the tolerance for many of the end-use applications identified by Deloitte [44], and the prediction errors for 316L stainless steel are acceptable for biomedical implant applications [43]. These high-quality predictions can also provide a means for practitioners to construct effective compensation plans for distortion control.

To further validate our methodology, we held out the 65 mm nominal diameter 316L stainless steel disk and used the remaining disks to train the distortion model. The same procedure as described in Sec. 3 was implemented. Once model transfer was completed by incorporating the TEA model into the baseline model, distortion predictions for the 65 mm nominal diameter disk were then obtained and compared to the observed distortions. The RMSE of distortion predictions for this 316 stainless steel disk is 19.8 μm, which is a relatively slight increase from the result in Table 3. This indicates that our model is effective for distortion prediction of new parts.

Our model transfer involved significantly less computational costs compared to a large number of existing finite element models. Specifically, transferring the distortion model from Ti–6Al–4V alloy to 316L stainless steel took a total of 45 min and 45 s on a 2015 MacBook Pro 2.2 GHz Intel Core i7 machine. If we assume a linear scale-up of the computation speed for FEA as reported in Refs. [19,51], then FEA would require over seven days of computation for each of the disks that we considered. It is important to note that the major computational costs for our method are incurred only when updating a model with new data. Minimal computational costs are incurred when making predictions for a new part under our method. For example, computation on the order of three seconds is incurred when making predictions for a new point cloud of 1.3×10^4 observations using our transferred model. The finite element model in Ref. [21] involves comparable computational time as that for performing the full model transfer in this application, but its disadvantage is that it takes this amount of time for each new part. A comparison of the accuracies of

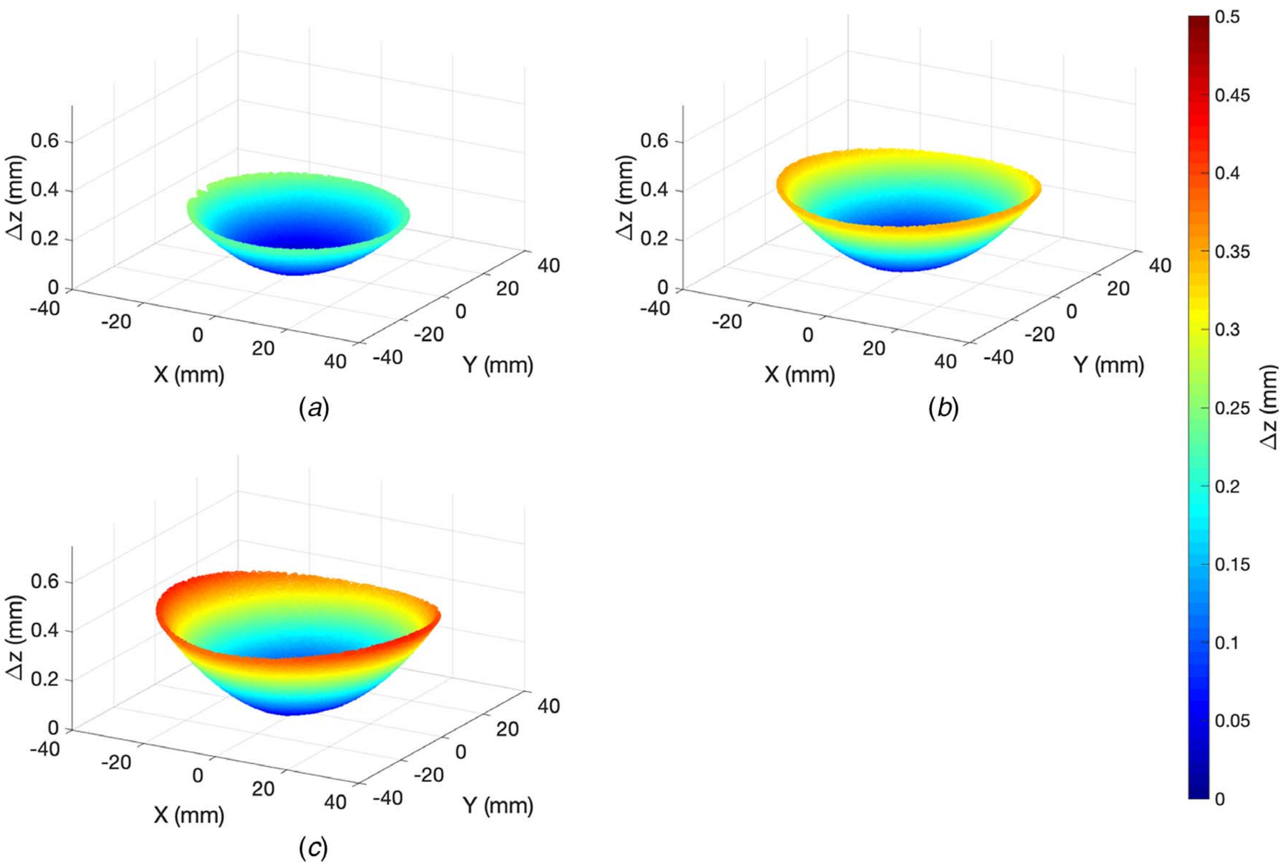

Fig. 10 Posterior predictive means of distortions derived from our transferred model for 316L stainless steel disks of nominal diameters (*a*) 55 mm, (*b*) 65 mm, and (*c*) 70 mm

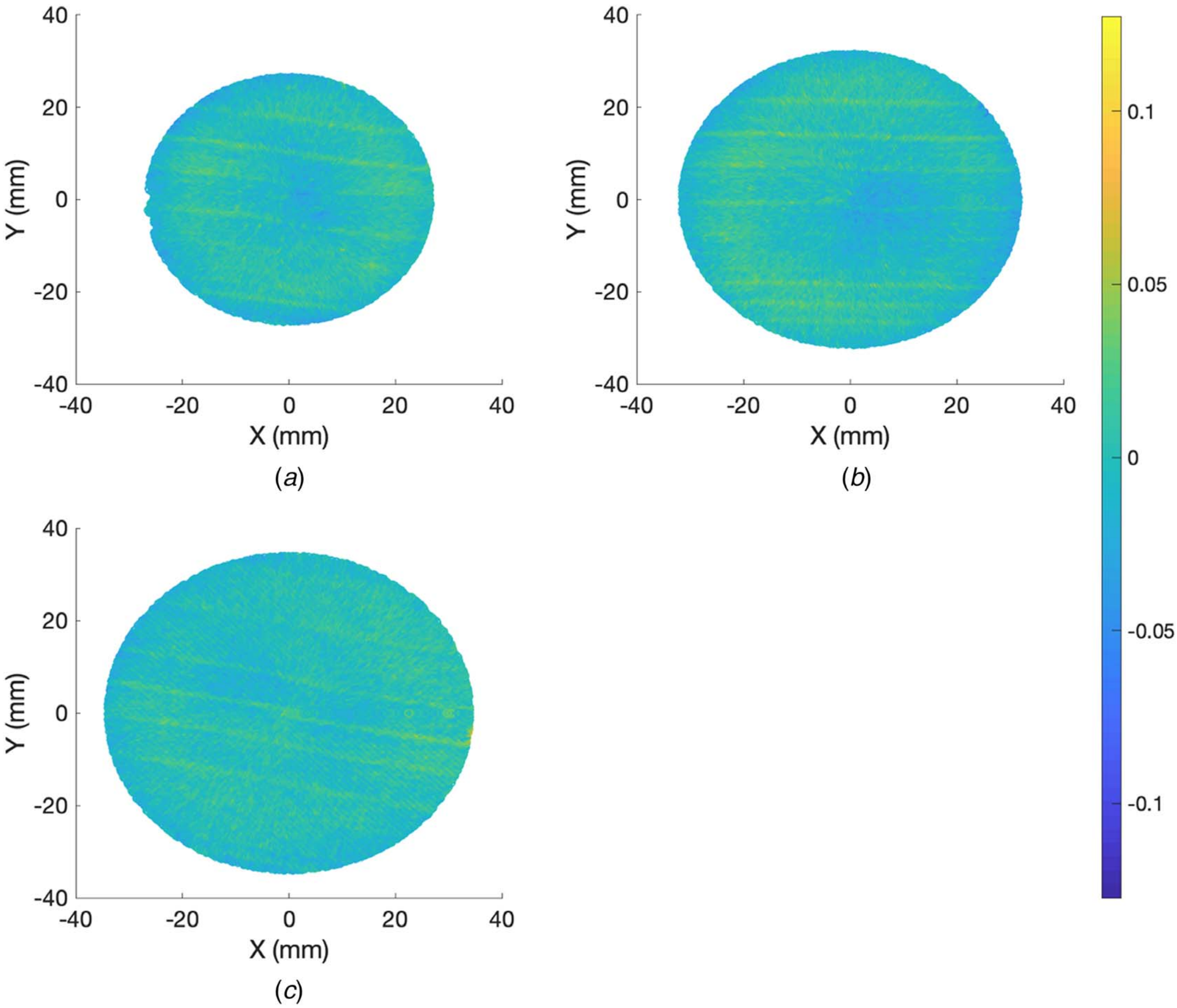

Fig. 11 Residuals of the transferred distortion model for the three 316L stainless steel disks with a thickness of 5 mm and nominal diameters (*a*) 55 mm, (*b*) 65 mm, and (*c*) 70 mm

distortion predictions between our model and that in Ref. [21] is not immediately available because the radius of curvature approach is used in Ref. [21] to fit a sphere to the distortion of the disk, whereas we directly use the pointwise distortion measurements obtained from the CMM. Model predictions given in Ref. [21] are reported to be within 20% of the true radius of curvature, whereas our distortion predictions are within 5% error of the measured distortion for all disks. A final point to note is that, as our method leverages past experiments, it can enable faster product certification of new material systems. Thus, another advantage of our method compared to existing FEA approaches, besides the smaller computational costs, is that the models obtained from our method possess the ability to continue learning and improving their fits via TEA models as more new parts are manufactured.

Table 3 RMSE, percent error, and worst case residual (i.e., the maximum of the absolute values of the residuals) for each disk's distortion predictions as obtained from our fitted models

Material	Nominal diameter (mm)	RMSE (μm)	Total distortion (μm)	Percent error (%)	Worst case residual (μm)
Ti–6Al–4V alloy	45	12.5	504	2.48	97.15
Ti–6Al–4V alloy	55	18.3	619	2.95	110.57
Ti–6Al–4V alloy	65	18.5	813	2.28	100.41
Ti–6Al–4V alloy	70	18.5	1071	1.73	127.22
316L stainless steel	55	12.7	302	4.21	54.23
316L stainless steel	65	13.9	380	3.66	65.32
316L stainless steel	70	11.8	500	2.36	65.29

5 Concluding Remarks

Laser-based additive manufacturing is a promising technology that can positively impact a wide range of potential applications, such as the manufacture of biomedical devices and aerospace components. However, an unfortunate feature of current research in LBAM is that a small number of materials are extensively studied within each distinct domain due to their particular advantageous properties for specific end-use applications. For example, Ti–6Al–4V alloy is the primary focus of study for the manufacture of biomedical devices due to its biocompatibility properties. A consequence of this is that much research is conducted that is heavily dependent on the selected materials. The model transfer methodology presented in this paper addresses this problem by bridging the gaps between different materials in LBAM. It does so by utilizing the effect equivalence framework in Ref. [1] to incorporate lurking differences in new material systems into a model that has already been specified for a previously studied material, so as to transfer that model to new materials. Bridging the gap between different materials in LBAM is made difficult by the significant differences in their properties. We demonstrated via our case study on distortions in Ti–6Al–4V and 316L stainless steel disks that this task is not only possible under our method, but that the transferred model for a new material can be of such high quality so as to meet end-use tolerances. To the best of our knowledge, our framework is the first to bridge the gaps between different material systems in LBAM.

Our model transfer method possesses multiple advantages for practitioners and researchers in LBAM.

(1) Its computational costs for distortion modeling and prediction are significantly less than those associated with most FEA approaches. This can enable practitioners and researchers to quickly test new materials for different end-use applications.
(2) It leverages past experiments and enables a distortion model to continuously learn and refine itself as more parts are manufactured. The latter features are made possible by our use of the Bayesian inferential paradigm. This advantage is particularly helpful for practitioners, who can better determine the necessary accuracy levels for specific applications. It also builds upon the smaller computational costs to further enable faster testing and product certification of new material systems with less expenditure of efforts and resources.
(3) Our model transfer method is not purely data-driven because it enables practitioners and researchers to directly incorporate physical parameters that are known to be significant into the transferred models. Other approaches cannot easily incorporate such parameters (e.g., thermal conductivity). These physical parameters are directly incorporated into the TEA model, and as more data are collected, additional physics-based knowledge can be incorporated.

Ultimately, our method can accelerate the study of many novel materials in LBAM, which previously may have been considered infeasible due to the extensive amount of computation or number of experiments that were thought necessary. The efficient use of past experiments and reduced costs for learning about new materials that result from our method can then lead to the identification of new application areas of LBAM and further advance the adoption of LBAM by industry. One possible example is the investigation of other Titanium alloys that may be more beneficial for specific biomedical implants. Today, Ti–6Al–4V alloy is mainly used for the fabrication of many biomedical implants, but through further material research, other alloys may be found to better suit specific individual biomedical implants, leading to greater patient satisfaction overall.

Future work includes the application of transferred distortion models for the construction of compensation plans in LBAM. By providing highly accurate distortion predictions based on data from different materials, more effective compensation plans can be derived under our method that ultimately improves the quality of additively manufactured parts. Further investigation is needed to validate the material transfer methodology for new material systems in LBAM. While our case study only shows the transfer from one material system to a second system, we believe that our methodology will work for other material systems. In general, the TEA model captures the difference between two material systems. By adding data from new material systems to refine the TEA model, the learning error will decrease and thus improve distortion predictions for a new material system. Another interesting avenue for future research is to investigate the interaction of thickness and diameter on the distortions of fabricated parts. Interestingly, the distortions of a 75 mm Ti–6Al–4V disk that was also manufactured was significantly different than the disks used in the case study. The cause of this is likely the large diameter-to-thickness ratio and will be explored in future work. Other quantities of interest, such as residual stress and geometric deviations in the (x, y) plane, could also be investigated using the proposed modeling framework. Multiple quantities of interest could be modeled simultaneously using a multivariate statistical distribution. Furthermore, with additional parts that possess varying geometries, the model may be generalized to predict distortions for many types of geometries instead of only the disks considered in this article. An example of a formulation that could be used for generalizing our model to various types of geometries can be found in Refs. [50,52]. The latter article suggests that the distortion models learned in our case study can serve to capture "global" distortion features that can be used to facilitate distortion modeling of more complicated shapes. An additional challenge for more complex parts is the introduction of cavities, which will alter distortion behaviors. Previous work [41] investigated cavities in small parts, but the methodology would likely need to be extended to account for cavities with larger volumes. Ultimately, our methodology provides a first step toward a more comprehensive distortion modeling framework of freeform shapes in LBAM.

Acknowledgment

This material is based upon work supported by the National Science Foundation under Grant No. CMMI-1544841 as part of the NSF/DHS/DOT/NASA/NIH Cyber-Physical Systems Program and Grant No. 1635966.

References

[1] Sabbaghi, A., and Huang, Q., 2018, "Model Transfer Across Additive Manufacturing Processes via Mean Effect Equivalence of Lurking Variables," Ann. Appl. Stat., **12**(4), pp. 2409–2429.
[2] Lee, J., Bagheri, B., and Kao, H.-A., 2015, "A Cyber-Physical Systems Architecture for Industry 4.0-Based Manufacturing Systems," Manuf. Lett., **3**(1), pp. 18–23.
[3] Baufeld, B., Van Der Biest, O., Gault, R., and Ridgway, K., 2011, "Manufacturing Ti–6Al–4V Components by Shaped Metal Deposition: Microstructure and Mechanical Properties," IOP Conference Series: Materials Science and Engineering, University of Sheffield, September, pp. 1–6.
[4] Carroll, B. E., Palmer, T. A., and Beese, A. M., 2015, "Anisotropic Tensile Behavior of Ti–6Al–4V Components Fabricated With Directed Energy Deposition Additive Manufacturing," Acta Mater., **87**(1), pp. 309–320.
[5] Helmer, H. E., Körner, C., and Singer, R. F., 2014, "Additive Manufacturing of Nickel-Based Superalloy Inconel 718 by Selective Electron Beam Melting: Processing Window and Microstructure," J. Mater. Res., **29**(17), pp. 1987–1996.
[6] Jia, Q., and Gu, D., 2014, "Selective Laser Melting Additive Manufacturing of Inconel 718 Superalloy Parts: Densification, Microstructure and Properties," J. Alloys Compd., **585**(1), pp. 713–721.
[7] Khairallah, S. A., Anderson, A. T., Rubenchik, A., and King, W. E., 2016, "Laser Powder-Bed Fusion Additive Manufacturing: Physics of Complex Melt Flow and Formation Mechanisms of Pores, Spatter, and Denudation Zones," Acta Mater., **108**(1), pp. 36–45.
[8] King, W. E., Barth, H. D., Castillo, V. M., Gallegos, G. F., Gibbs, J. W., Hahn, D. E., Kamath, C., and Rubenchik, A. M., 2014, "Observation of Keyhole-Mode Laser Melting in Laser Powder-Bed Fusion Additive Manufacturing," J. Mater. Process. Technol., **214**(12), pp. 2915–2925.
[9] Thijs, L., Verhaeghe, F., Craeghs, T., Humbeeck, J. V., and Kruth, J. P., 2010, "A Study of the Microstructural Evolution During Selective Laser Melting of Ti–6Al–4V," Acta Mater., **58**(9), pp. 3303–3312.
[10] Tian, Y., McAllister, D., Colijn, H., Mills, M., Farson, D., Nordin, M., and Babu, S., 2014, "Rationalization of Microstructure Heterogeneity in Inconel 718 Builds Made by the Direct Laser Additive Manufacturing Process," Metall. Mater. Trans. A, **45**(10), pp. 4470–4483.
[11] Wu, A. S., Brown, D. W., Kumar, M., Gallegos, G. F., and King, W. E., 2014, "An Experimental Investigation Into Additive Manufacturing-Induced Residual Stresses in 316L Stainless Steel," Metall. Mater. Trans. A, **45**(13), pp. 6260–6270.
[12] Wei, C., Sun, Z., Chen, Q., Liu, Z., and Li, L., 2019, "Additive Manufacturing of Horizontal and 3D Functionally Graded 316L/Cu10Sn Components via Multiple Material Selective Laser Melting," ASME J. Manuf. Sci. Eng., **141**(8), p. 081014.
[13] Huang, J., Xu, Z., Deng, Y., and Peng, L., 2019, "Electropulsing-Induced to Phase Transformation of Ti–6Al–4V," ASME J. Manuf. Sci. Eng., **141**(11), p. 111012.
[14] ASM Aerospace Specification Materials Inc., 2018, "Titanium Ti–6Al–4V (Grade 5), Annealed," Pompano Beach, FL.
[15] AK Steel, 2016, "316/316L Stainless Steel." Tech. Rep., AK Steel, West Chester, OH.
[16] Dunbar, A. J., Denlinger, E. R., Heigel, J., Michaleris, P., Guerrier, P., Martukanitz, R., and Simpson, T. W., 2016, "Development of Experimental

Method for In Situ Distortion and Temperature Measurements During the Laser Powder Bed Fusion Additive Manufacturing Process," Addit. Manuf., **12**(A), pp. 25–30.
[17] Roberts, I. A., 2012, "Investigation of Residual Stresses in the Laser Melting of Metal Powders in AM," Ph.D. thesis, University of Wolverhampton, Wolverhampton.
[18] Paul, R., Anand, S., and Gerner, F., 2014, "Effect of Thermal Deformation on Part Errors in Metal Powder Based Additive Manufacturing Processes," ASME J. Manuf. Sci. Eng., **136**(3), p. 031009.
[19] Mukherjee, T., Zuback, J. S., De, A., and DebRoy, T., 2016, "Printability of Alloys for Additive Manufacturing," Sci. Rep., **6**(1), pp. 1–8.
[20] Peng, H., Ghasri-Khouzani, M., Gong, S., Attardo, R., Ostiguy, P., Gatrell, B. A., Budzinski, J., Tomonto, C., Neidig, J., Shankar, M. R., Billo, R., Go, D. B., and Hoelzle, D., 2018, "Fast Prediction of Thermal Distortion in Metal Powder Bed Fusion Additive Manufacturing: Part 1, a Thermal Circuit Network Model," Addit. Manuf., **22**(1), pp. 852–868.
[21] Peng, H., Ghasri-Khouzani, M., Gong, S., Attardo, R., Ostiguy, P., Rogge, R. B., Gatrell, B. A., Budzinski, J., Tomonto, C., Neidig, J., Shankar, M. R., Billo, R., Go, D. B., and Hoelzle, D., 2018, "Fast Prediction of Thermal Distortion in Metal Powder Bed Fusion Additive Manufacturing: Part 2, a Quasi-Static Thermo-Mechanical Model," Addit. Manuf., **22**(1), pp. 869–882.
[22] Denlinger, E. R., Heigel, J. C., Michaleris, P., and Palmer, T. A., 2015, "Effect of Inter-Layer Dwell Time on Distortion and Residual Stress in Additive Manufacturing of Titanium and Nickel Alloys," J. Mater. Process. Technol., **215**(1), pp. 123–131.
[23] Corbin, D. J., Nassar, A. R., Reutzel, E. W., Beese, A. M., and Michaleris, P., 2018, "Effect of Substrate Thickness and Preheating on the Distortion of Laser Deposited Ti–6Al–4V," ASME J. Manuf. Sci. Eng., **140**(6), p. 061009.
[24] Levkulich, N., Semiatin, S., Gockel, J., Middendorf, J., DeWald, A., and Klingbeil, N., 2019, "The Effect of Process Parameters on Residual Stress Evolution and Distortion in the Laser Powder Bed Fusion of Ti–6Al–4V," Addit. Manuf., **28**(1), pp. 475–484.
[25] Ghasri-Khouzani, M., Peng, H., Rogge, R., Attardo, R., Ostiguy, P., Neidig, J., Billo, R., Hoelzle, D., and Shankar, M. R., 2017, "Experimental Measurement of Residual Stress and Distortion in Additively Manufactured Stainless Steel Components With Various Dimensions," Mater. Sci. Eng. A, **707**(11), pp. 689–700.
[26] Pan, S. J., and Yang, Q., 2010, "A Survey on Transfer Learning," IEEE Trans. Knowl. Data Eng., **22**(10), pp. 1345–1359.
[27] Dai, W., Yang, Q., Xue, G.-R., and Yu, Y., 2007, "Boosting for Transfer Learning," Proceedings of the 24th International Conference on Machine Learning, Oregon State University, June, pp. 193–200.
[28] Pardoe, D., and Stone, P., 2010, "Boosting for Regression Transfer," Proceedings of the 27th International Conference on Machine Learning, Haifa, Israel, June 2010, pp. 863–870.
[29] Weiss, K., Khoshgoftaar, T. M., and Wang, D., 2016, "A Survey of Transfer Learning," J. Big Data, **3**(1), pp. 1–40.
[30] Day, O., and Khoshgoftaar, T. M., 2017, "A Survey on Heterogeneous Transfer Learning," J. Big Data, **4**(1), pp. 1–42.
[31] Raina, P., Battle, A., Lee, H., Packer, B., and Ng, A., 2007, "Self-Taught Learning: Transfer Learning From Unlabeled Data," Proceedings of the 24th International Conference Machine Learning, Oregon State University, June 2007, pp. 759–766.
[32] Pearl, J., and Bareinboim, E., 2014, "External Validity: From Do-Calculus to Transportability Across Populations," Stat. Sci., **29**(4), pp. 579–595.
[33] Bareinboim, E., and Pearl, J., 2016, "Causal Inference and the Data-Fusion Problem," Proceedings of the National Academy of Sciences, **113**(27), pp. 7345–7352.
[34] Pearl, J., 1995, "Causal Diagrams for Empirical Research," Biometrika, **82**(4), pp. 669–688.
[35] Aboutaleb, A. M., Bian, L., Elwany, A., Shamsaei, N., Thompson, S. M., and Tapia, G., 2017, "Accelerated Process Optimization for Laser-Based Additive Manufacturing by Leveraging Similar Prior Studies," IISE Trans., **49**(1), pp. 31–44.
[36] Joseph, V. R., Dasgupta, T., Tuo, R., and Wu, C. J., 2015, "Sequential Exploration of Complex Surfaces Using Minimum Energy Designs," Technometrics, **57**(1), pp. 64–74.
[37] Wang, H., Huang, Q., and Katz, R., 2005, "Multi-Operational Machining Processes Modeling for Sequential Root Cause Identification and Measurement Reduction," ASME Trans. J. Manuf. Sci. Eng., **127**(3), pp. 512–521.
[38] Wang, H., and Huang, Q., 2006, "Error Cancellation Modeling and Its Application in Machining Process Control," IIE Trans. Qual. Reliab., **38**(4), pp. 379–388.
[39] Wang, H., and Huang, Q., 2007, "Using Error Equivalence Concept to Automatically Adjust Discrete Manufacturing Processes for Dimensional Variation Control," ASME Trans. J. Manuf. Sci. Eng., **129**(3), pp. 644–652.
[40] Huang, Q., and Wang, H., 2008, "Error Equivalence Methodology for Dimensional Variation Control in Manufacturing," 2008 IEEE Conference on Robotics, Automation and Mechatronics, Chengdu, China, September 2008, pp. 1–6.
[41] Sabbaghi, A., and Huang, Q., 2016, "Predictive Model Building Across Different Process Conditions and Shapes in 3D Printing," 2016 IEEE International Conference on Automation Science and Engineering (CASE 2016), Fort Worth, TX, August 2016, pp. 774–779.
[42] Ferreira, R., Sabbaghi, A., and Huang, Q., 2019, "Automated Geometric Shape Deviation Modeling for Additive Manufacturing Systems via Bayesian Neural Networks," IEEE Trans. Autom. Sci. Eng., pp. 1–15.
[43] Malaguti, G., Denti, L., Bassoli, E., Franchi, I., Bortolini, S., and Gatto, A., 2011, "Dimensional Tolerances and Assembly Accuracy of Dental Implants and Machined Versus Cast-On Abutments," Clin. Implant Dent. Relat. Res., **13**(2), pp. 134–140.
[44] Coykendall, J., Cotteleer, M., Holdowsky, L., and Mahto, M., 2014, *3D Opportunity in Aerospace and Defense*, Deloitte University Press, Deloitte: New York, pp. 1–28.
[45] Huang, Q., Zhang, J., Sabbaghi, A., and Dasgupta, T., 2015, "Optimal Offline Compensation of Shape Shrinkage for 3D Printing Processes," IIE Trans. Qual. Reliab., **47**(5), pp. 431–441.
[46] Rubin, D. B., 1984, "Bayesianly Justifiable and Relevant Frequency Calculations for the Applied Statistician," Ann. Stat., **12**(4), pp. 1151–1172.
[47] Meng, X.-L., 1994, "Posterior Predictive *p*-values," Ann. Stat., **22**(3), pp. 1142–1160.
[48] Gelman, A., Meng, X.-L., and Stern, H., 1996, "Posterior Predictive Assessment of Model Fitness via Realized Discrepancies," Stat. Sin., **6**(4), pp. 733–807.
[49] Sabbaghi, A., Dasgupta, T., Huang, Q., and Zhang, J., 2014, "Inference for Deformation and Interference in 3D Printing," Ann. Appl. Stat., **8**(3), pp. 1395–1415.
[50] Sabbaghi, A., Huang, Q., and Dasgupta, T., 2018, "Bayesian Model Building From Small Samples of Disparate Data for Capturing In-Plane Deviation in Additive Manufacturing," Technometrics, **60**(4), pp. 532–544.
[51] Mukherjee, T., Manvatkar, V., De, A., and DebRoy, T., 2017, "Mitigation of Thermal Distortion During Additive Manufacturing," Scr. Mater., **127**(1), pp. 79–83.
[52] Luan, H., Grasso, M., Colosimo, B. M., and Huang, Q., 2019, "Prescriptive Data-Analytical Modeling of Laser Powder Bed Fusion Processes for Accuracy Improvement," ASME J. Manuf. Sci. Eng., **141**(1), p. 011008.